Sensitivity of a homogeneous and isotropic second-gradient continuum model for particle-based materials with respect to uncertainties

Gabriele La Valle, Bilen Emek Abali, Giovanni Falsone, Christian Soize

Sensitivity of a homogeneous and isotropic second-gradient continuum model for particle-based materials with respect to uncertainties

Gabriele La Valle [*1,2,4], Bilen Emek Abali[3], Giovanni Falsone[1], and Christian Soize[4]

[1]University of Messina, Department of Engineering, C.da Di Dio, 98158 Messina, Italy.

[2]International Research Center M&MoCS, University of L'Aquila, L'Aquila, Italy.

[3]Uppsala University, Division of Applied Mechanics, Box 35, 751 03 Uppsala, Sweden.

[4]Université Gustave Eiffel, MSME UMR 8208, 5 bd Descartes, 77454 Marne-la-Vallée, France.

May 13, 2023

Abstract

This work concerns the probabilistic analysis of particle-based materials. More precisely, this work is devoted to the stochastic modeling of the geometric and constitutive microscale parameters associated with particle-pair interactions of an existing model for particle-based materials. Such an issue is addressed with a probabilistic methodology that relies on the maximum entropy principle from information theory. After defining and improving the chosen second-gradient continuum model for particle-based materials, it is shown that for micro-homogeneous and micro-isotropic materials, the involved microscale parameters turn out to be statistically independent. More precisely, the particle-pair distance between two consecutive particles is a uniformly distributed random variable and the specific microscale stiffness parameters are Gamma-distributed random variables. A homogeneous and isotropic 2D concrete plate subjected to an axial load is considered for illustration purposes. A stochastic solver based on Monte Carlo numerical simulations and mixed finite element (FE) method are chosen. The FE discretization is applied to the weak formulation of the equivalent continuum model with random mechanical properties. On the contrary, the particle-pair distance and the microscale stiffness parameters, which are the parameters of the boundary value problem formulated for the equivalent continuum model, are modeled as random variables. Finally, uncertainties propagation is discussed and statistical fluctuations of the macro mechanical response are found to be significant.

*Corresponding Author. *gablavalle@unime.it*

1 Introduction

Particle-based materials consist of an assembly of a great number of rigid particles with arbitrary shapes. For such complex systems, several discrete and equivalent continuum models have been proposed in the literature. In the last decades, numerous efforts have been made for improving the continuum-based approaches. The use of the generalized continuum theories has been proposed that enrich the classical ones with scale parameters related to particle-pair interactions. Among others, we mention nonlocal continuum theories, micropolar continuum theories and second-gradient continuum theories.

Nonlocal continuum theories differ from classical ones because the constitutive equations relating stress and strain are nonlocal. First works on the topic are found in [28, 26, 22], where continuum models able to take into account finite range interaction forces are developed. Recent theoretical and numerical developments are presented in [23]. In [7, 8, 9], applications concerning the failure of heterogeneous materials and the modeling of strain-softening are proposed.

Micropolar continuum theories are possibly traced back to [14] that summarizes the main concepts discussed at the end of nineteenth century by Kelvin, Helmholtz, Duhem, Voigt, Le Roux, the Cosserats and others [6]. From a kinematic point of view, micropolar continuum theories add an independent rotational field to the displacement field considered in classical continuum theories. Recent results are given in [21, 5]. Nowadays, micropolar continuum theories are used to model several phenomena in solid and fluid mechanics [35]. In [31], a micropolar elastic model for soils is formulated that overcomes the numerical difficulties encountered in the failure analysis performed within the framework of classical continuum theories. In [33], a rigid-plastic micropolar model is used for slow frictional flow of particle-based materials in order to predict experimental evidences for cylindrical Couette flow.

Second gradient theories are characterized by deformation energy functionals depending on the first and second order derivatives of the displacement field. Moreover, they are characterized by unusual boundary conditions whose physical significance is addressed and clarified in [19, 20]. Precursor of second-gradient theories is Gabrio Piola whose works are summarized in [15, 18]. Second gradient theories are currently applied for describing the mechanical behaviors of metamaterials. A paradigmatic case is represented by pantographic structures [17, 3, 13, 42]. Nevertheless, their use in technical contexts is limited by several difficulties related to the experimental identification of second-order constitutive parameters, which is usually performed with arbitrary simplifications [4, 30, 45]. In [32, 10], a particle-based second-gradient continuum model is proposed that overcomes the above mentioned deficiency. It allows us to express the second-gradient constitutive parameters in terms of relatively few microscale geometric and constitutive parameters related to the particle-pair interaction. Recent applications of this model concern the analysis of damage of particle-based materials by following a hemivariational approach [43, 36].

The studies cited so far are deterministic. Material properties fail to be deterministic in reality and uncertainties have to be taken into account. Uncertainty quantification is important to correctly estimate mechanical responses

of media made up of particle-based materials. A review of stochastic methods of analysis of particle-based-effects uncertainties at the microscale on their response at the macroscale is given in [34] within the framework of first gradient continuum theories. Nevertheless, despite the intrinsic random nature of particle-based materials, uncertainties have not still been taken into account within the framework of second-gradient continuum theories. Recently, few studies involving some uncertain quantities have been proposed in the context of second-gradient theories, not for particle-based, but for fiber materials [12, 37] and for pantographic structures [44, 29].

This work provides for the first time a study of the second-gradient continuum model for particle-based materials derived from [36, 10] in accounting for uncertainties and, more generally, for uncertainty quantification of a second-gradient continuum model for particle-based materials. The analyzed model could be also applied to two-phase composite materials with rigid inclusion and to granular materials. The application of this modeling to composite materials with rigid inclusion is immediate. On the contrary, if we wish to apply this modeling to granular materials, hypotheses should be added concerning the topology of contacts between contiguous grains, granulometry involved, grain sizes, grain shapes, and granular matter configurations. Moreover, assumptions should be added concerning the geometric disorder and structure of granular materials.

This paper is organized as follows. In Section 2, the deterministic second-gradient continuum model for particle-based materials developed in [36, 10] is used and the analytical relationship between the first- and second-gradient deformation tensors is modified for improving the algebraic derivation. Section 3 is devoted to the definition of the corresponding random second-gradient continuum model for particle-based materials. Under the hypotheses of micro-homogeneity and micro-isotropy, the prior probabilistic distributions for the involved geometric and constitutive microscale parameters are derived and discussed through the maximum entropy principle. Although the equivalent continuum model is derived from the discrete one, this is not a classical homogenization problem for which there is a microstructure that is a random medium represented by apparent mechanical properties and a macrostructure with effective mechanical properties that would be deterministic for scale separation. For the sake of simplicity, in Section 4, the stochastic boundary value (BVP) problem is introduced in the context of the application and not in a general framework. A derived stochastic computational model is constructed by means of the mixed finite element (FE) method [38, 25] with the aid of open-source packages developed under the FEniCS project. The FE discretization is applied to the weak formulation of the equivalent continuum model with deterministic geometry. The only sources of uncertainty are the particle-pair distance and microscale stiffness parameters, which are the BVP parameters that model material cohesion by describing particle interactions. As a consequence, the convergence with respect to the FE size mesh is not related to the random properties of the analyzed system. For uncertainty-propagation analysis, a stochastic solver based on Monte Carlo numerical simulation is used whose convergence is studied. Finally, for this type of particle-based mechanical medium, a discussion on uncertainties propagation is presented.

Notation

A lower case letter such as x, η, u is a real deterministic variable except when used as an integer index as i, j, etc. Greek letters α, β, η and τ are either deterministic variables or integers as subscripts.

A boldface lower case letter such as $\boldsymbol{x}$, $\boldsymbol{\eta}$, $\boldsymbol{u}$ is a real deterministic vector.

An upper case letter such as X, H, U is a real random variable except when used as an integer index as A, B, etc.

A boldface upper case letter such as $\boldsymbol{X}$, $\boldsymbol{H}$, $\boldsymbol{U}$ is a vector random variable.

A lower case letter between brackets such as $[x]$, $[\eta]$, $[u]$ is a real deterministic second-order tensor.

A boldface upper case letter between brackets such as $[\boldsymbol{X}]$, $[\boldsymbol{H}]$, $[\boldsymbol{U}]$ is a real random second-order tensor.

A lower case Gothic letter between brackets such as $[\mathfrak{x}]$, $[\mathfrak{h}]$, $[\mathfrak{u}]$ is a real deterministic third-order tensor.

A boldface upper case Gothic letter between brackets such as $[\boldsymbol{\mathfrak{X}}]$, $[\boldsymbol{\mathfrak{H}}]$, $[\boldsymbol{\mathfrak{U}}]$ is a real random third-order tensor.

A lower case letter between two brackets such as $[[x]]$, $[[z]]$, $[[u]]$ is a real deterministic fourth-order tensor.

A lower case Gothic letter between two brackets such as $[[\mathfrak{x}]]$, $[[\mathfrak{h}]]$, $[[\mathfrak{u}]]$ is a real deterministic fifth-order tensor.

A lower case letter between three brackets such as $[[[x]]]$, $[[[h]]]$, $[[[u]]]$ is a real deterministic sixth-order tensor.

$\mathbb{E}$: Mathematical expectation.

The Levi-Civita tensor calculus is used. Indices denoted by upper case letters are chosen to indicate components in the initial configuration and lowercase letters to indicate components in the current configuration. Summation over the repeated Latin indices is used. There is no summation over repeated Greek indices. Superscripts denote the contravariant components, and subscripts denote the covariant ones.

$\|\boldsymbol{x}\|$: Euclidean norm of $\boldsymbol{x} \in \mathbb{R}^n$

$\|A\|$: $\mathrm{Sup}_{\|\boldsymbol{x}\|\leq 1} \|A\boldsymbol{x}\|$ operator norm of linear operator A.

$[g]$: metric tensor.

$[\delta]$: Kronecker delta.

$[x]^T$: transpose of the second-order tensor $[x]$, and $\left[x^T\right]$ is the second-order tensor of the transposition.

$\mathbb{1}_B$: indicator function of a set B.

2 Defining a deterministic particle-based continuum

2.1 Discrete model

We summarize the model proposed in [10, 43, 36]. Let β be a rigid particle and let us build a discrete set of n rigid particles at distance ℓ from β (same arguments can be generalized for ℓ variable along the spatial directions). Let us consider the discrete system of rigid particles obtained by assembling s of these sets. It is a discrete grid of rigid particles within a bounded domain $\mathcal{L}$ of $\mathbb{R}^3$ such that the distance between two consecutive particles in the grid is ℓ. Although any particle shape is acceptable, particle sizes must be sufficiently small to justify the passage from the discrete to the equivalent continuum model in Subsection 2.2. Let α and β be two consecutive particles in the grid, whose coordinate vectors are $\boldsymbol{q}_\alpha = (q^1_\alpha, q^2_\alpha, q^3_\alpha)$ and $\boldsymbol{q}_\beta = (q^1_\beta, q^2_\beta, q^3_\beta)$ in a given fixed coordinate system defined by a generic basis of $\mathbb{R}^3$. We define $\boldsymbol{r} = (r^1, r^2, r^3) : \boldsymbol{q} \mapsto r(\boldsymbol{q})$ as the configuration function and we introduce the second-order tensor valued-function $[f]$ such as

$$[f] : \boldsymbol{q} \mapsto [f(\boldsymbol{q})] = \{[f(\boldsymbol{q})]^i_A = \frac{\partial r^i(\boldsymbol{q})}{\partial q^A}, i = 1,2,3; A = 1,2,3\} \tag{1}$$

and we define $[f_\beta] = [f(\boldsymbol{q}_\beta)]$. Let $\boldsymbol{u}_{\alpha\beta}$ be the objective deformation vector such that [1]

$$\boldsymbol{u}_{\alpha\beta} = \left[f^T_\beta\right] \left(\boldsymbol{r}\left(\boldsymbol{q}_\alpha\right) - \boldsymbol{r}\left(\boldsymbol{q}_\beta\right)\right) - \left(\boldsymbol{q}_\alpha - \boldsymbol{q}_\beta\right). \tag{2}$$

Truncated at the second-order, the Taylor expansion of $\boldsymbol{r}$ in the neighborhood of $\boldsymbol{q}_\beta$ yields

$$r^i\left(\boldsymbol{q}_\alpha\right) \approx r^i\left(\boldsymbol{q}_\beta\right) + \left.\frac{\partial r^i(\boldsymbol{q})}{\partial q^A}\right|_{\boldsymbol{q}=\boldsymbol{q}_\beta} \left(q^A_\alpha - q^A_\beta\right) + \frac{1}{2} \left.\frac{\partial^2 r^i(\boldsymbol{q})}{\partial q^A \partial q^B}\right|_{\boldsymbol{q}=\boldsymbol{q}_\beta} \left(q^A_\alpha - q^A_\beta\right)\left(q^B_\alpha - q^B_\beta\right). \tag{3}$$

Let $\widehat{\boldsymbol{n}}_{\alpha\beta}$ be the unit vector defining the orientation of one pair (α, β) of two consecutive particles such as

$$\boldsymbol{q}_\alpha - \boldsymbol{q}_\beta = \widehat{\boldsymbol{n}}_{\alpha\beta}\, \ell. \tag{4}$$

Substituting Eqs. (3) and (4) in Eq. (2) yields

$$\begin{aligned} u^C_{\alpha\beta} &= \left[f^T_\beta\right]^C_i \left(\left[f^T_\beta\right]^i_B \widehat{n}^B_{\alpha\beta}\, \ell + \frac{1}{2} \left.\frac{\partial^2 r^i(\boldsymbol{q})}{\partial q^A \partial q^B}\right|_{\boldsymbol{q}=\boldsymbol{q}_\beta} \widehat{n}^B_{\alpha\beta}\, \ell\, \widehat{n}^A_{\alpha\beta}\, \ell \right) - [\delta]^C_B\, \widehat{n}^B_{\alpha\beta}\, \ell \\ &= \left(\left[f^T_\beta\right]^C_i \left[f^T_\beta\right]^i_B - [\delta]^C_B \right) \left(\widehat{n}^B_{\alpha\beta}\, \ell\right) + \frac{1}{2} \left[f^T_\beta\right]^C_i \left.\frac{\partial^2 r^i(\boldsymbol{q})}{\partial q^A \partial q^B}\right|_{\boldsymbol{q}=\boldsymbol{q}_\beta} \widehat{n}^B_{\alpha\beta}\, \widehat{n}^A_{\alpha\beta}\, \ell^2. \end{aligned} \tag{5}$$

[1] In components: $u^C_{\alpha\beta} = \left[f^T_\beta\right]^C_i \left(r^i\left(\boldsymbol{q}_\alpha\right) - r^i\left(\boldsymbol{q}_\beta\right)\right) - \left(q^C_\alpha - q^C_\beta\right)$

Let us define the two deformation tensors $[e] : \boldsymbol{q} \mapsto [e](\boldsymbol{q})$ and $[\mathfrak{h}] : \boldsymbol{q} \mapsto [\mathfrak{h}](\boldsymbol{q})$ such that

$$[e]_B^C = \frac{1}{2}\left([f]_i^C \left[f^T\right]_B^i - [\delta]_B^C\right), \tag{6}$$

$$[\mathfrak{h}]_{AB}^C = \left[f^T\right]_i^C \frac{\partial^2 r^i}{\partial q^A \partial q^B}. \tag{7}$$

We introduce the notation $[e_\beta] = [e](\boldsymbol{q}_\beta)$ and $[\mathfrak{h}_\beta] = [\mathfrak{h}](\boldsymbol{q}_\beta)$. The tensor $[e]$ is the Cauchy–Green tensor. Substituting Eqs. (6) and (7) into Eq. (5) yields

$$\begin{aligned} u_{\alpha\beta}^C = 2\,[e_\beta]_B^C\,\widehat{n}_{\alpha\beta}^B\,\ell + \frac{1}{2}\left[f_\beta^T\right]_i^C \left.\frac{\partial^2 r^i(\boldsymbol{q})}{\partial q^A \partial q^B}\right|_{\boldsymbol{q}=\boldsymbol{q}_\beta} \widehat{n}_{\alpha\beta}^B\,\widehat{n}_{\alpha\beta}^A\,\ell^2 = \\ = 2\,[e_\beta]_B^C\,\widehat{n}_{\alpha\beta}^B\,\ell + \frac{1}{2}\,[\mathfrak{h}_\beta]_{AB}^C\,\widehat{n}_{\alpha\beta}^B\,\widehat{n}_{\alpha\beta}^A\,\ell^2. \end{aligned} \tag{8}$$

Equation (7) can be written (see [16]) as

$$[\mathfrak{h}_\beta]_{AB}^C = \frac{1}{2}\,[g]^{DC}\left(\left.\frac{\partial\,[e]_{AD}(\boldsymbol{q})}{\partial q^B}\right|_{\boldsymbol{q}=\boldsymbol{q}_\beta} + \left.\frac{\partial\,[e]_{BD}(\boldsymbol{q})}{\partial q^A}\right|_{\boldsymbol{q}=\boldsymbol{q}_\beta} - \left.\frac{\partial\,[e]_{BA}(\boldsymbol{q})}{\partial q^D}\right|_{\boldsymbol{q}=\boldsymbol{q}_\beta}\right). \tag{9}$$

Let us define the elastic energy function $\Delta w_{\alpha\beta} : \boldsymbol{u}_{\alpha\beta} \mapsto \Delta w_{\alpha\beta}(\boldsymbol{u}_{\alpha\beta})$ related to the interaction of the pair (α, β). Since $\boldsymbol{u}_{\alpha\beta}$ is an objective function, it is considered as a measure of deformation (see Eq. (2)). Among all possible choices for the function $\Delta w_{\alpha\beta}$, it is chosen such that

$$\Delta w_{\alpha\beta}(\boldsymbol{u}_{\alpha\beta}) = \Delta w_{\alpha\beta\eta}(\boldsymbol{u}_{\alpha\beta}) + \Delta w_{\alpha\beta\tau}(\boldsymbol{u}_{\alpha\beta}), \tag{10}$$

in which

$$\Delta w_{\alpha\beta\eta}(\boldsymbol{u}_{\alpha\beta}) = \frac{1}{2}\,k_{\alpha\beta\eta}\,\|\boldsymbol{u}_{\alpha\beta\eta}\|^2 \quad , \quad \Delta w_{\alpha\beta\tau}(\boldsymbol{u}_{\alpha\beta}) = \frac{1}{2}\,k_{\alpha\beta\tau}\,\|\boldsymbol{u}_{\alpha\beta\tau}\|^2, \tag{11}$$

and where

$$\boldsymbol{u}_{\alpha\beta\eta} = \frac{1}{2}\,(\boldsymbol{u}_{\alpha\beta}\cdot\widehat{\boldsymbol{n}}_{\alpha\beta})\,\widehat{\boldsymbol{n}}_{\alpha\beta} \quad , \quad \boldsymbol{u}_{\alpha\beta\tau} = \boldsymbol{u}_{\alpha\beta} - (\boldsymbol{u}_{\alpha\beta}\cdot\widehat{\boldsymbol{n}}_{\alpha\beta})\,\widehat{\boldsymbol{n}}_{\alpha\beta}, \tag{12}$$

in which $k_{\alpha\beta\eta}$ and $k_{\alpha\beta\tau}$ are two given positive local microscale constitutive parameters, and in which $\boldsymbol{u}_{\alpha\beta\eta}$ and $\boldsymbol{u}_{\alpha\beta\tau}$ are the vector decomposition of the deformation vector $\boldsymbol{u}_{\alpha\beta}$ parallel and orthogonal to $\widehat{\boldsymbol{n}}_{\alpha\beta}$, respectively. The vector decomposition of $\boldsymbol{u}_{\alpha\beta}$ in $2\boldsymbol{u}_{\alpha\beta\eta}$ and $\boldsymbol{u}_{\alpha\beta\tau}$ with respect to the local coordinates system $\left(q^{1(\mathrm{lc})}, q^{2(\mathrm{lc})}, q^{3(\mathrm{lc})}\right)$ is shown in Fig. 1. For technical needs, no coupling energetic term, such as $\|\boldsymbol{u}_{\alpha\beta\eta}\|\,\|\boldsymbol{u}_{\alpha\beta\tau}\|$, is considered between $\boldsymbol{u}_{\alpha\beta\eta}$ and $\boldsymbol{u}_{\alpha\beta\tau}$. It allows us to state a relationship between the microscale constitutive parameters, $k_{\alpha\beta\eta}$ and $k_{\alpha\beta\tau}$, and the macroscale constitutive parameters, and to obtain an equivalent second-gradient continuum model for particle-based based materials that generalizes the classical (or Cauchy) continuum model. The energy Δw_β

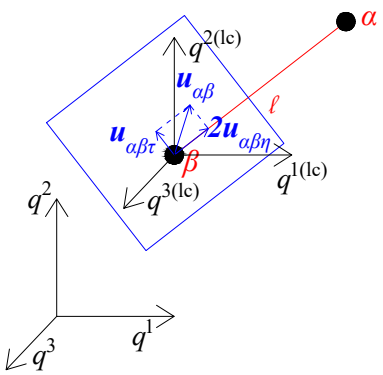

Figure 1: Vector decomposition of $\boldsymbol{u}_{\alpha\beta}$ in the local coordinates system $\boldsymbol{q}^{(\mathrm{lc})} = \left(q^{1(\mathrm{lc})}, q^{2(\mathrm{lc})}, q^{3(\mathrm{lc})}\right)$, in which $2\boldsymbol{u}_{\alpha\beta\eta}$ is the projection of $\boldsymbol{u}_{\alpha\beta}$ with respect to $\widehat{\boldsymbol{n}}_{\alpha\beta}$ and $\boldsymbol{u}_{\alpha\beta\tau}$ is the projection on the plane defined by $\boldsymbol{u}_{\alpha\beta}$ and $\boldsymbol{u}_{\alpha\tau}$. Particles can have different sizes and different shapes. Any particle shape is admissible. Particle sizes need to be small enough to pass from the discrete to the equivalent continuum model. The quantities $\boldsymbol{u}_{\alpha\beta}$, $\boldsymbol{u}_{\alpha\beta\eta}$, $\boldsymbol{u}_{\alpha\beta\tau}$ have been defined in Eqs. (7) and (12). They represent deformation measures of the particle-pair (α,β).

due to the interactions between all the n consecutive particles of β, labeled as 1_β,...,n_β, is written as

$$\Delta w_\beta = \sum_{\alpha=1_\beta}^{n_\beta} \Delta w_{\alpha\beta}\left(\boldsymbol{u}_{\alpha\beta}\right) = \sum_{\alpha=1_\beta}^{n_\beta} \left(\frac{1}{2}\, k_{\alpha\beta\eta} \left\| \boldsymbol{u}_{\alpha\beta\eta} \right\|^2 + \frac{1}{2}\, k_{\alpha\beta\tau} \left\| \boldsymbol{u}_{\alpha\beta\tau} \right\|^2 \right), \tag{13}$$

Finally, the total energy w related to the considered system of particles is equal to

$$w = \sum_{\beta=1}^{s} \sum_{\alpha=1_\beta}^{n_\beta} \Delta w_{\alpha\beta} = \sum_{\beta=1}^{s} \sum_{\alpha=1_\beta}^{n_\beta} \left(\frac{1}{2} k_{\alpha\beta\eta} \left\| \boldsymbol{u}_{\alpha\beta\eta} \right\|^2 + \frac{1}{2} k_{\alpha\beta\tau} \left\| \boldsymbol{u}_{\alpha\beta\tau} \right\|^2 \right). \tag{14}$$

2.2 Equivalent continuum model

If the distance ℓ between two consecutive particles is small enough with respect to the smaller characteristic dimension of domain $\mathcal{L}$, we can replace the discrete model by an equivalent continuum model. Let $\widehat{\boldsymbol{n}} : \boldsymbol{\omega} \mapsto \widehat{\boldsymbol{n}}\left(\boldsymbol{\omega}\right)$ be the orientation field in which $\boldsymbol{\omega} \in \Omega = [0, 2\pi] \times [0, 2\pi]$ and let $\boldsymbol{u} : \boldsymbol{q} \mapsto \boldsymbol{u}\left(\boldsymbol{q}\right)$ such that

$$\begin{aligned} u^C(\boldsymbol{q}, \boldsymbol{\omega}) = 2\, [e]_B^C(\boldsymbol{q})\, \widehat{n}^B(\boldsymbol{\omega})\, \ell + \frac{1}{2}\, \left[f^T(\boldsymbol{q})\right]_i^C \frac{\partial^2 r^i(\boldsymbol{q})}{\partial q^A \partial q^B} \widehat{n}^B(\boldsymbol{\omega})\, \widehat{n}^A(\boldsymbol{\omega})\, \ell^2 = \\ = 2\, [e]_B^C(\boldsymbol{q})\, \widehat{n}^B(\boldsymbol{\omega})\, \ell + \frac{1}{2}\, [\mathfrak{h}]_{AB}^C(\boldsymbol{q})\, \widehat{n}^B(\boldsymbol{\omega})\, \widehat{n}^A(\boldsymbol{\omega})\, \ell^2. \end{aligned} \tag{15}$$

For the continuum model, the deformation energy w is written as

$$w = \int_{\mathcal{L}} \phi\left(\boldsymbol{q}\right)\, d\boldsymbol{q} = \int_{\mathcal{L}} \int_{\Omega} \psi\left(\boldsymbol{\omega}, \boldsymbol{q}\right)\, d\boldsymbol{\omega}\, d\boldsymbol{q} = \int_{\mathcal{L}} \int_{\Omega} \left(\frac{1}{2}\, \widetilde{k}_\eta\left(\boldsymbol{\omega}, \boldsymbol{q}\right)\, \left\| \boldsymbol{u}_\eta\left(\boldsymbol{\omega}, \boldsymbol{q}\right) \right\|^2 + \frac{1}{2}\, \widetilde{k}_\tau\left(\boldsymbol{\omega}, \boldsymbol{q}\right)\, \left\| \boldsymbol{u}_\tau\left(\boldsymbol{\omega}, \boldsymbol{q}\right) \right\|^2 \right) d\boldsymbol{\omega}\, d\boldsymbol{q}, \tag{16}$$

where $\phi : \boldsymbol{q} \mapsto \phi(\boldsymbol{q})$ is the specific deformation energy and $\psi : (\boldsymbol{\omega}, \boldsymbol{q}) \mapsto \psi(\boldsymbol{\omega}, \boldsymbol{q})$ is the specific deformation energy per unit direction, such that

$$\phi(\boldsymbol{q}) = \int_{\Omega} \psi(\boldsymbol{\omega}, \boldsymbol{q}) \, d\boldsymbol{\omega}, \quad \psi(\boldsymbol{\omega}, \boldsymbol{q}) = \frac{1}{2} \widetilde{k}_{\eta}(\boldsymbol{\omega}, \boldsymbol{q}) \, \|\boldsymbol{u}_{\eta}(\boldsymbol{\omega}, \boldsymbol{q})\|^2 + \frac{1}{2} \widetilde{k}_{\tau}(\boldsymbol{\omega}, \boldsymbol{q}) \, \|\boldsymbol{u}_{\tau}(\boldsymbol{\omega}, \boldsymbol{q})\|^2, \tag{17}$$

in which $\boldsymbol{u}_{\eta} : (\boldsymbol{\omega}, \boldsymbol{q}) \mapsto \boldsymbol{u}_{\eta}(\boldsymbol{\omega}, \boldsymbol{q})$ and $\boldsymbol{u}_{\tau} : \boldsymbol{q} \mapsto \boldsymbol{u}_{\tau}(\boldsymbol{\omega}, \boldsymbol{q})$ are such that

$$\boldsymbol{u}_{\eta}(\boldsymbol{\omega}, \boldsymbol{q}) = \frac{1}{2} (\boldsymbol{u}(\boldsymbol{q}) \cdot \widehat{\boldsymbol{n}}(\boldsymbol{\omega})) \, \widehat{\boldsymbol{n}}(\boldsymbol{\omega}) \quad , \quad \boldsymbol{u}_{\tau}(\boldsymbol{\omega}, \boldsymbol{q}) = \boldsymbol{u}(\boldsymbol{q}) - \boldsymbol{u}_{\eta}(\boldsymbol{\omega}, \boldsymbol{q}). \tag{18}$$

The mappings $\widetilde{k}_{\eta} : (\boldsymbol{\omega}, \boldsymbol{q}) \mapsto \widetilde{k}_{\eta}(\boldsymbol{\omega}, \boldsymbol{q})$ and $\widetilde{k}_{\tau} : (\boldsymbol{\omega}, \boldsymbol{q}) \mapsto \widetilde{k}_{\tau}(\boldsymbol{\omega}, \boldsymbol{q})$ are the specific stiffness fields per unit direction. The specific deformation energy $\phi(\boldsymbol{q})$ is written as

$$\phi(\boldsymbol{q}) = \frac{1}{2} \, [[c]]^{BL}_{CM}(\boldsymbol{q}) \, [e]^{C}_{B}(\boldsymbol{q}) \, [e]^{M}_{L}(\boldsymbol{q}) + \frac{1}{2} \, [[\mathfrak{c}]]^{BEF}_{CD}(\boldsymbol{q}) \, [e]^{C}_{B}(\boldsymbol{q}) \, [\mathfrak{h}]^{D}_{EF}(\boldsymbol{q}) + \frac{1}{2} \, [[[a]]]^{ABFL}_{CM}(\boldsymbol{q}) \, [\mathfrak{h}]^{C}_{AB}(\boldsymbol{q}) \, [\mathfrak{h}]^{M}_{FL}(\boldsymbol{q}), \tag{19}$$

in which $[[c]]$, $[[[a]]]$ and $[[\mathfrak{c}]]$ are the constitutive tensors that are detailed in [10] and where $[[c]]$ is the classical constitutive tensor.

2.3 Case of a homogeneous and isotropic equivalent continuum model

Let us call "micro-homogeneous" a continuum characterized by constant specific microscale stiffness fields along spatial direction $\boldsymbol{q}$, *i.e.*, $\widetilde{k}_{\eta}(\boldsymbol{\omega}, \boldsymbol{q}) = \widetilde{k}^{(hom)}_{\eta}(\boldsymbol{\omega})$ and $\widetilde{k}_{\tau}(\boldsymbol{\omega}, \boldsymbol{q}) = \widetilde{k}^{(hom)}_{\tau}(\boldsymbol{\omega})$. Let us call "micro-isotropic" a continuum in which the specific microscale stiffness fields are constant along the direction of interaction $\boldsymbol{\omega}$, *i.e*, $\widetilde{k}_{\eta}(\boldsymbol{\omega}, \boldsymbol{q}) = k^{(iso)}_{\eta}(\boldsymbol{q})$ and $\widetilde{k}_{\tau}(\boldsymbol{\omega}, \boldsymbol{q}) = k^{(iso)}_{\tau}(\boldsymbol{q})$. If the continuum is micro-homogeneous and micro-isotropic, we have $\widetilde{k}_{\eta}(\boldsymbol{\omega}, \boldsymbol{q}) = k_{\eta}$ and $\widetilde{k}_{\tau}(\boldsymbol{\omega}, \boldsymbol{q}) = k_{\tau}$, where k_{η} and k_{τ} belongs to $\mathbb{R}^+$. At the macroscale, choosing the coordinate system defined by the canonical (or standard) basis of $\mathbb{R}^3$, it is proven in [10, 43, 36] that the homogeneous and isotropic continuum is characterized by the specific deformation energy $\phi(\boldsymbol{q})$ defined by

$$\begin{aligned} \phi(\boldsymbol{q}) = \xi_2 \, [e]^{A}_{B}(\boldsymbol{q}) \, [e]^{B}_{A}(\boldsymbol{q}) + \frac{1}{2} \xi_1 \, [e]^{A}_{A}(\boldsymbol{q}) \, [e]^{B}_{B}(\boldsymbol{q}) + \\ + 2 \xi_3 \, [\mathfrak{h}]^{A}_{AB}(\boldsymbol{q}) \, [\mathfrak{h}]^{B}_{CC}(\boldsymbol{q}) + \frac{1}{2} \xi_4 \, [\mathfrak{h}]^{A}_{AB}(\boldsymbol{q}) \, [\mathfrak{h}]^{C}_{CB}(\boldsymbol{q}) + \\ + 2 \xi_5 \, [\mathfrak{h}]^{A}_{BA}(\boldsymbol{q}) \, [\mathfrak{h}]^{B}_{CC}(\boldsymbol{q}) + \xi_6 \, [\mathfrak{h}]^{A}_{BC}(\boldsymbol{q}) \, [\mathfrak{h}]^{A}_{BC}(\boldsymbol{q}) + 2 \xi_7 \, [\mathfrak{h}]^{A}_{BC}(\boldsymbol{q}) \, [\mathfrak{h}]^{C}_{AB}(\boldsymbol{q}). \end{aligned} \tag{20}$$

The symbols ξ_1 and ξ_2 are the Lamé coefficients in classical elasticity. The term homogeneous is used here to underline that ξ_1, ξ_2,..., and ξ_7 are constant. The term isotropic is used here to underline that the specific deformation energy is invariant under coordinate rotation (see [2] for more details). By adding the hypotheses of micro-isotropic

and micro-homogeneous continua, the functions $\widehat{\xi}_1$ and $\widehat{\xi}_2$ are defined by

$$\xi_1 = \widehat{\xi}_1(\ell, k_\eta, k_\tau) = \frac{4\pi\,\ell^2}{15}(k_\eta - 4k_\tau) \quad , \quad \xi_2 = \widehat{\xi}_2(\ell, k_\eta, k_\tau) = \frac{4\pi\,\ell^2}{15}(k_\eta + 6k_\tau). \tag{21}$$

The remaining parameters ξ_3, ξ_4, ξ_5, ξ_6 and ξ_7 depend on ξ_1 and ξ_2, which, in turn depend on ℓ, k_η and k_τ,

$$\xi_3 = \widehat{\xi}_3(\ell, k_\eta, k_\tau) = \frac{\ell^2}{112}\widehat{\xi}_1(\ell, k_\eta, k_\tau) = \xi_4 \quad , \quad \xi_5 = \widehat{\xi}_5(\ell, k_\eta, k_\tau) = \frac{\ell^2}{1120}\Big(7\widehat{\xi}_2(\ell, k_\eta, k_\tau) + 3\widehat{\xi}_1(\ell, k_\eta, k_\tau)\Big) = \xi_7, \tag{22}$$

$$\xi_6 = \widehat{\xi}_6(\ell, k_\eta, k_\tau) = \frac{\ell^2}{1120}\Big(7\widehat{\xi}_2(\ell, k_\eta, k_\tau) - 4\widehat{\xi}_1(\ell, k_\eta, k_\tau)\Big). \tag{23}$$

In the following, a probabilistic model is proposed for ℓ, k_η and k_τ under the hypotheses of micro-homogeneity and micro-isotropy. Then, the random mechanical response of continua described by Eqs. (20), (22), and (23) is studied.

3 Defining the random particle-based continuum

Let $\boldsymbol{X} : \theta \mapsto \boldsymbol{X}(\theta) = (L(\theta), K_\eta(\theta), K_\tau(\theta))$ be the random variable with values in $\mathbb{R}^3$, defined on the probability space $(\Theta, \mathcal{T}, \mathcal{P})$, whose probability distribution is $P_{\boldsymbol{X}}$ on $\mathbb{R}^3$. The random variable L describes the random particle-pair distance between two consecutive particles, K_η and K_τ are the random microscale stiffness fields modeling interactions between two consecutive particles. Under the hypotheses of micro-homogeneity and micro-isotropy, L, K_η, and K_τ are assumed to be independent of the spatial and orientation directions. Equation (21) allows us to define the random variables $\Xi_1 : \theta \mapsto \Xi_1(\theta) = \widehat{\xi}_1(L(\theta), K_\eta(\theta), K_\tau(\theta))$ and $\Xi_2 : \theta \mapsto \Xi_2(\theta) = \widehat{\xi}_2(L(\theta), K_\eta(\theta), K_\tau(\theta))$ such that

$$\Xi_1 = \frac{4\pi L^2}{15}(K_\eta - 4K_\tau) \quad , \quad \Xi_2 = \frac{4\pi L^2}{15}(K_\eta + 6K_\tau), \tag{24}$$

The symbols Ξ_1 and Ξ_2 correspond to the random Lamé coefficients in classical elasticity. Equations (22) and (23) lead us to define the random variables $\Xi_3 = \Xi_4 : \theta \mapsto \Xi_3(\theta) = \Xi_4(\theta) = \widehat{\xi}_3(L(\theta), K_\eta(\theta), K_\tau(\theta))$, $\Xi_5 : \theta \mapsto \Xi_5(\theta) = \Xi_7(\theta) = \widehat{\xi}_5(L(\theta), K_\eta(\theta), K_\tau(\theta))$ and $\Xi_6 : \theta \mapsto \Xi_6(\theta) = \widehat{\xi}_6(L(\theta), K_\eta(\theta), K_\tau(\theta))$.

At $\boldsymbol{q}$, the random specific deformation energy $\Phi(\boldsymbol{q}) : \theta \mapsto \Phi(\boldsymbol{q}, \theta)$ is obtained by substituting the deterministic quantities $(\xi_1, \xi_2, [\boldsymbol{e}](\boldsymbol{q}), [\mathfrak{h}](\boldsymbol{q}))$ in Eq. (20) by the random ones $(\Xi_1(\theta), \Xi_2(\theta), [\boldsymbol{E}](\boldsymbol{q}, \theta), [\mathfrak{H}](\boldsymbol{q}, \theta))$, and is given by

$$\begin{aligned}\Phi(\boldsymbol{q}) = \Xi_2\,[E]^A_B(\boldsymbol{q})\,[E]^B_A(\boldsymbol{q}) + \frac{1}{2}\Xi_1\,[E]^A_A(\boldsymbol{q})\,[E]^B_B(\boldsymbol{q}) + \\ +2\,\Xi_3\,[\mathfrak{H}]^A_{AB}(\boldsymbol{q})\,[\mathfrak{H}]^B_{CC}(\boldsymbol{q}) + \frac{1}{2}\Xi_4\,[\mathfrak{H}]^A_{AB}(\boldsymbol{q})\,[\mathfrak{H}]^C_{CB}(\boldsymbol{q}) + \\ +2\,\Xi_5\,[\mathfrak{H}]^A_{BA}(\boldsymbol{q})\,[\mathfrak{H}]^B_{CC}(\boldsymbol{q}) + \Xi_6\,[\mathfrak{H}]^A_{BC}(\boldsymbol{q})\,[\mathfrak{H}]^A_{BC}(\boldsymbol{q}) + 2\,\Xi_7\,[\mathfrak{H}]^A_{BC}(\boldsymbol{q})\,[\mathfrak{H}]^C_{AB}(\boldsymbol{q}),\end{aligned} \tag{25}$$

where $[\boldsymbol{E}](\boldsymbol{q}) : \theta \mapsto [\boldsymbol{E}](\boldsymbol{q}, \theta)$ is the random Cauchy–Green deformation tensor and $[\mathfrak{H}](\boldsymbol{q}) : \theta \mapsto [\mathfrak{H}](\boldsymbol{q}, \theta)$ is the random second-gradient deformation tensor, which depend on the random configuration function $\boldsymbol{R} : \theta \mapsto \{\boldsymbol{q} \mapsto$

$\boldsymbol{R}(\boldsymbol{q},\theta)\}$. The random deformation energy per unit direction, $\Psi(\boldsymbol{\omega},\boldsymbol{q}) : \theta \mapsto \Psi(\boldsymbol{\omega},\boldsymbol{q},\theta)$, is given by

$$\Psi(\boldsymbol{\omega},\boldsymbol{q}) = \frac{1}{2} K_\eta \left\| \boldsymbol{U}_\eta(\boldsymbol{\omega},\boldsymbol{q}) \right\|^2 + \frac{1}{2} K_\tau \left\| \boldsymbol{U}_\tau(\boldsymbol{\omega},\boldsymbol{q}) \right\|^2, \tag{26}$$

in which

$$\boldsymbol{U}_\eta(\boldsymbol{\omega},\boldsymbol{q}) = \frac{1}{2} \left(\boldsymbol{U}(\boldsymbol{q}) \cdot \widehat{\boldsymbol{n}}(\boldsymbol{\omega}) \right) \widehat{\boldsymbol{n}}(\boldsymbol{\omega}) \quad , \quad \boldsymbol{U}_\tau(\boldsymbol{\omega},\boldsymbol{q}) = \boldsymbol{U}(\boldsymbol{q}) - \boldsymbol{U}_\eta(\boldsymbol{\omega},\boldsymbol{q}), \tag{27}$$

and where $\boldsymbol{U} : \theta \mapsto \{\boldsymbol{q} \mapsto \boldsymbol{U}(\boldsymbol{q},\theta)\}$ is the random field defined by

$$\begin{aligned} U^C(\boldsymbol{q}) = 2\, [E]^C_B(\boldsymbol{q})\, \widehat{n}^B(\boldsymbol{\omega})\, \ell + \frac{1}{2}\, \left[F^T(\boldsymbol{q})\right]^C_i \frac{\partial^2 R^i(\boldsymbol{q})}{\partial q^A \partial q^B}\, \widehat{n}^B(\boldsymbol{\omega})\, \widehat{n}^A(\boldsymbol{\omega})\, \ell^2 = \\ = 2\, [E]^C_B(\boldsymbol{q})\, \widehat{n}^B(\boldsymbol{\omega})\, \ell + \frac{1}{2}\, [\mathfrak{H}]^C_{AB}(\boldsymbol{q})\, \widehat{n}^B(\boldsymbol{\omega})\, \widehat{n}^A(\boldsymbol{\omega})\, \ell^2, \end{aligned} \tag{28}$$

where $[\boldsymbol{F}(\boldsymbol{q})] : \theta \mapsto [\boldsymbol{F}(\boldsymbol{q})](\theta) = \{[F(\boldsymbol{q})]^i_A(\theta) = \frac{\partial R^i(\boldsymbol{q},\theta)}{\partial q^A}, i = 1,2,3\,; A = 1,2,3\}$. The approach proposed in [27] for classical linear elasticity is used in Subsection 3.2. In Subsection 3.1, the maximum entropy principle is used to define a prior probability model for $\boldsymbol{X} = (L, K_\eta, K_\tau)$, which are the only source of uncertainty of the continuum model under consideration. In the spirit of the previous deterministic model, since we analyze the equivalent continuum model, the geometry of the single rigid particles, which are modeled as material points, are not considered here. The connectivity of the particles is modeled by means of the microscale stiffness parameters K_η and K_τ. The random variables L, K_η, and K_τ are assumed to be independent of spatial and orientation directions. If we wish to apply the exposed second-gradient continuum model for particle-based materials to granular materials, as for the deterministic case, remarks should be added concerning the geometry and shapes of the grains, granulometry involved, geometry disorder, and structure of the granular medium. The application is immediate for composite materials.

3.1 Maximum entropy principle for constructing the prior probability distribution of uncertain parameters

The Shannon entropy $\mathcal{E}(p_{\boldsymbol{X}})$ of a probability density function (pdf) $p_{\boldsymbol{X}}$ on $\mathbb{R}^n$ is defined by
$\mathcal{E}(p_{\boldsymbol{X}}) = -\int_{\mathbb{R}^n} p_{\boldsymbol{X}}(\boldsymbol{x}) \log\left(p_{\boldsymbol{X}}(\boldsymbol{x})\right) d\boldsymbol{x}$, which measures the level of uncertainties. Higher uncertainty results in a larger Shannon entropy.

In accordance with the maximum entropy (MaxEnt) principle, the pdf of the $\mathbb{R}^3$-valued random variable $\boldsymbol{X} = (L, K_\eta, K_\tau)$ maximizes the Shannon entropy under the constraints defined by the available information (see for instance [41]) that are given as follows:

(Q1) The support of $p_{\boldsymbol{X}}$ is

$$\operatorname{Supp} p_{\boldsymbol{X}} = \mathcal{S}_{\boldsymbol{X}} \quad , \quad \mathcal{S}_{\boldsymbol{X}} \subseteq [\zeta_1, \zeta_2] \times \mathbb{R}^+ \times \mathbb{R}^+ \subset \mathbb{R}^3, \tag{29}$$

where $0 < \zeta_1 < \zeta_2 < +\infty$.

(Q2) The mean value of K_η and K_τ are given and finite,

$$\mathbb{E}\{K_\eta\} = \gamma_\eta < +\infty \quad , \quad \gamma_\eta \in \mathbb{R}^+, \tag{30}$$

$$\mathbb{E}\{K_\tau\} = \gamma_\tau < +\infty \quad , \quad \gamma_\tau \in \mathbb{R}^+. \tag{31}$$

(Q3) The inverse of the random matrix $[\boldsymbol{K}]$ such that

$$[\boldsymbol{K}] = \begin{bmatrix} K_\eta & 0 \\ 0 & K_\tau \end{bmatrix}, \tag{32}$$

has a finite second-order moment (for physical consistencies),

$$\mathbb{E}\left\{\left\|\boldsymbol{K}^{-1}\right\|^2\right\} < +\infty. \tag{33}$$

This property can be stated as suggested in [39, 40] and can be replaced by the following one: the random variable $\log(\det([\boldsymbol{K}]))$ has a given mean value whose absolute value is finite,

$$\mathbb{E}\{\log(\det([\boldsymbol{K}]))\} = \gamma_{\det} \quad , \quad |\gamma_{\det}| < +\infty. \tag{34}$$

Since the random variable $\det([\boldsymbol{K}]) = K_\eta\, K_\tau$, Eq. (34) can be rewritten as

$$\mathbb{E}\{\mu(K_\eta, K_\tau)\} = \gamma_{\det} \quad , \quad \mu(K_\eta, K_\tau) = \log(K_\eta\, K_\tau)\ . \tag{35}$$

We now consider the $\mathbb{R}^2$-valued random variable (K_η, K_τ) defined on $(\Theta, \mathcal{T}, \mathcal{P})$. The constraints stated by propositions (Q2) and (Q3) read

$$\mathbb{E}\{\boldsymbol{h}(K_\eta, K_\tau)\} = \boldsymbol{\gamma}, \tag{36}$$

where $\boldsymbol{\gamma} = (\gamma_\eta, \gamma_\tau, \gamma_{\det})$ and $\boldsymbol{h} : \mathbb{R}^2 \mapsto \mathbb{R}^3$ such that

$$\boldsymbol{h}(k_\eta, k_\tau) = (k_\eta, k_\tau, \log(k_\eta\, k_\tau)). \tag{37}$$

Let $\mathcal{C}_{\text{free}}$ (see [41]) be the set of functions on $\mathbb{R}^3$, defined by

$$\mathcal{C}_{\text{free}} = \left\{p \in L^1\left(\mathbb{R}^3, \mathbb{R}^+\right), \text{Supp } p = \mathcal{S}_{\boldsymbol{X}}\right\}. \tag{38}$$

The set $\mathcal{C}_{\text{ad}}$ of the admissible probability density functions $p : (\ell, k_\eta, k_\tau) \mapsto p(\ell, k_\eta, k_\tau)$ of $\boldsymbol{X} = (L, K_\eta, K_\tau)$ is defined by

$$\mathcal{C}_{\text{ad}} = \left\{ p \in \mathcal{C}_{\text{free}},\ \int_{\mathbb{R}^3} p\left(\ell, k_\eta, k_\tau\right)\, d\ell\, dk_\eta\, dk_\tau = 1,\ \int_{\mathbb{R}^3} \boldsymbol{h}\left(k_\eta, k_\tau\right) p\left(\ell, k_\eta, k_\tau\right)\, d\ell\, dk_\eta\, dk_\tau = \boldsymbol{\gamma} \right\}. \tag{39}$$

Under the constraints defined by (Q1), (Q2), and (Q3), and using the MaxEnt principle, it is possible to prove that pdf $p_{\boldsymbol{X}}$ of $\boldsymbol{X}$ is the unique solution to the following optimization problem,

$$p_{\boldsymbol{X}} = \arg\max_{p \in \mathcal{C}_{\text{ad}}} \mathcal{E}\left(p\right), \tag{40}$$

where $p \mapsto \mathcal{E}(p)$ is the Shannon entropy defined by

$$\mathcal{E}(p) = -\int_{\mathbb{R}^3} p\left(\ell, k_\eta, k_\tau\right) \log\left(p\left(\ell, k_\eta, k_\tau\right)\right)\, d\ell\, dk_\eta\, dk_\tau. \tag{41}$$

3.2 Effective construction of the prior probability distribution of uncertain parameters

Proposition 1 *For the micro-homogeneous and micro-isotropic continuum in the field of the particle-based theory presented in Section 2, the expression of the joint probability density function of the random variables L, K_η, and K_τ, constructed using the maximum entropy (MaxEnt) principle under the constraints defined by (Q1), (Q3), and (Q3), shows that random variables L, K_η and K_τ are statistically independent. It also shows that the random variable L is uniformly distributed in $[\zeta_1, \zeta_2]$, and that K_η and K_τ are Gamma distributed in $\mathbb{R}^+$, whose parameters are*

$$(\alpha_\eta, \beta_\eta) = \left(1 - \lambda_c, \frac{m_{K_\eta}}{1 - \lambda_c}\right) \quad \text{and} \quad (\alpha_\tau, \beta_\tau) = \left(1 - \lambda_c, \frac{m_{K_\tau}}{1 - \lambda_c}\right). \tag{42}$$

In Eq. (42), $m_{K_\eta} = \mathbb{E}\left\{K_\eta\right\}$ and $m_{K_\tau} = \mathbb{E}\left\{K_\tau\right\}$ are the given mean values of K_η and K_τ, and $\lambda_c \in\,]-\infty, 1[$ controls the statistical fluctuations. The parameters $(\alpha_\eta, \beta_\eta)$ and $(\alpha_\tau, \beta_\tau)$ can be expressed as a function of the mean values m_{K_η} and m_{K_τ} and of the coefficients of variation $\text{cv}_{K_\eta} = \sigma_{K_\eta}/m_{K_\eta}$ and $\text{cv}_{K_\tau} = \sigma_{K_\tau}/m_{K_\tau}$ of K_η and of K_τ,

$$m_{K_\eta} = \alpha_\eta \beta_\eta \quad , \quad m_{K_\tau} = \alpha_\tau \beta_\tau \quad , \quad \text{cv}_{K_\eta} = \text{cv}_{K_\tau} = \frac{1}{\sqrt{1 - \lambda_c}}. \tag{43}$$

Note that the statistical fluctuations of K_η and K_τ, which are driven by their coefficients of variation, depend only on the same single parameter λ_c.

Proof The following proof is inspired from [27]. The solution of the optimization problem defined by Eq. (40) is written as

$$p_{L\, K_\eta\, K_\tau}\left(\ell, k_\eta, k_\tau\right) = \mathbb{1}_{\mathcal{S}_{\boldsymbol{X}}}\left(\ell, k_\eta, k_\tau\right) c_0^{\text{sol}} \exp(-\langle \boldsymbol{\lambda}^{\text{sol}}, \boldsymbol{h}\left(k_\eta, k_\tau\right)\rangle) \quad , \quad \forall\left(\ell, k_\eta, k_\tau\right) \in \mathbb{R}^3, \tag{44}$$

where $\boldsymbol{h} : \mathbb{R}^2 \mapsto \mathbb{R}^3$ is such that $\boldsymbol{h}(k_\eta, k_\tau) = (k_\eta, k_\tau, \log(k_\eta\, k_\tau))$ (see Eq. (37)), the positive normalization constant

c_0^{sol} and the Lagrange multiplier $\boldsymbol{\lambda}^{\text{sol}} = (\lambda_\eta, \lambda_\tau, \lambda_c)$ are such that $p_{L\,K_\eta\,K_\tau}$ belongs to the admissible set $\mathcal{C}_{\text{ad}}$ defined by Eq. (39). An algebraic calculation shows that the support $\mathcal{S}_{\boldsymbol{X}}$ introduced in Eq. (29) can be written as $\mathcal{S}_{\boldsymbol{X}} = [\zeta_1, \zeta_2] \times \mathbb{R}^+ \times \mathbb{R}^+$ and that, substuiting Eq. (37) into (44), $p_{L\,K_\eta\,K_\tau}$ can be written as

$$p_{L\,K_\eta\,K_\tau}(\ell, k_\eta, k_\tau) = p_L(\ell)\; p_{K_\eta}(k_\eta)\; p_{K_\tau}(k_\tau) \tag{45}$$

in which

$$p_L(\ell) = \mathbb{1}_{[\zeta_1,\zeta_2]}(\ell)\; c_1, \tag{46}$$

$$p_{K_\eta}(k_\eta) = \mathbb{1}_{\mathbb{R}^+}(k_\eta)\; c_2\, k_\eta^{-\lambda_c} \exp\{-\lambda_\eta\, k_\eta\}, \tag{47}$$

and

$$p_{K_\tau}(k_\tau) = \mathbb{1}_{\mathbb{R}^+}(k_\tau)\; c_3\, k_\tau^{-\lambda_c} \exp\{-\lambda_\tau\, k_\tau\}, \tag{48}$$

where c_1, c_2, and c_3 are positive normalization constants such that $c^{\text{sol}} = c_1\, c_2\, c_3$. As a consequence, the random variables L, K_η and K_τ are statistically independent. Hence, L is uniformly distributed, K_η and K_τ are Gamma distributed with parameters $(\alpha_\eta, \beta_\eta) = (1 - \lambda_c, 1/\lambda_\eta)$ and $(\alpha_\tau, \beta_\tau) = (1 - \lambda_c, 1/\lambda_\tau)$. Since

$$1 = \int_{[\zeta_1,\zeta_2]} \mathbb{1}_{[\zeta_1,\zeta_2]}(\ell)\; c_1\, dl = c_1\,(\zeta_2 - \zeta_1), \tag{49}$$

$$1 = c_2 \int_{\mathbb{R}^+} k_\eta^{-\lambda_c} \exp\{-\lambda_\eta k_\eta\}\; dk_\eta = c_2 \frac{\Gamma(1-\lambda_c)}{\lambda_\eta^{1-\lambda_c}}, \tag{50}$$

$$1 = c_2 \int_{\mathbb{R}^+} k_\tau^{-\lambda_c} \exp\{-\lambda_\tau k_\tau\}\; dk_\tau = c_2 \frac{\Gamma(1-\lambda_c)}{\lambda_\tau^{1-\lambda_c}}, \tag{51}$$

where $\Gamma : z \mapsto \Gamma(z) = \int_0^{+\infty} s^{z-1} \exp(-s)\, ds$ is the Gamma function. The normalization constants are found to be

$$c_1 = \frac{1}{\zeta_2 - \zeta_1} \quad , \quad c_2 = \frac{\lambda_\eta^{1-\lambda_c}}{\Gamma(1-\lambda_c)} \quad , \quad c_3 = \frac{\lambda_\tau^{1-\lambda_c}}{\Gamma(1-\lambda_c)}, \tag{52}$$

while it can be deduced that $1/\lambda_\eta = m_{K_\eta}/(1-\lambda_c)$ and $1/\lambda_\tau = m_{K_\tau}/(1-\lambda_c)$. To guarantee the finite value of the integrals in Eqs. (50) and (51), we must have $1 - \lambda_c > 0$, $\lambda_\eta > 0$ and $\lambda_\tau > 0$. Using the argument presented in Appendix B of [27], it can be seen that this algebraic solution is the unique solution of the optimization problem defined by Eq. (39).

Let us emphasize that the outcomes presented in this section are the result of applying the MaxEnt principle with the available information (Q1), (Q2), and (Q3).

4 Stochastic boundary value problem and its random solution defined in the application framework

To simplify the presentation, for constructing and analyzing the boundary value problem (BVP) for the random particle-based continuum model exposed in Section 3, the methodology is directly applied to a composite sample and not presented in a general case. We consider a plate with a hole placed in the middle whose mechanical properties are those of concrete and that is subjected to a numerical axial traction test. The domain of this plate is denoted by $\mathcal{L}$ and its boundary is $\partial\mathcal{L} = \partial\mathcal{L}_0 \cup \partial\mathcal{L}_t \cup \partial\mathcal{L}_1$. A zero Dirichlet condition is applied on $\partial\mathcal{L}_0$ (left end), where the body is clamped. A Neumann boundary condition is applied on $\partial\mathcal{L}_t$ (right end), where the uniaxial traction is applied. The displacement field is free on $\partial\mathcal{L}_1$ (see Fig. 2).

4.1 Geometry, load, deterministic and random mechanical properties

The values of the geometry parameters defined in Fig. (2) are $b_1 = 3\times10^{-1}\,m$, $b_2 = 5\times10^{-2}\,\mathrm{m}$, and $b_3 = 1\times10^{-2}\,\mathrm{m}$. The amplitude of the uniaxial traction load is $t = 1.5\times10^{9}\,\mathrm{N/m^2}$. The mean values $m_{\Xi_1} = \mathbb{E}\{\Xi_1\}$ and $m_{\Xi_2} = \mathbb{E}\{\Xi_2\}$ of the random Lamé coefficients Ξ_1 and Ξ_2 are such that $m_{\Xi_1} = 3.529\times10^{9}\,\mathrm{N/m^2}$ and $m_{\Xi_2} = 10^{10}\,\mathrm{N/m^2}$. Using Eq. (24) and because L is independent on K_η and K_τ, then, solving the linear equations for the mean values of K_η and K_τ yields

$$m_{K_\eta} = \mathbb{E}\{K_\eta\} = 8.613\times10^{15}\,\mathrm{N/m^4} \quad , \quad m_{K_\tau} = \mathbb{E}\{K_\tau\} = 1.029\times10^{15}\,\mathrm{N/m^4}. \tag{53}$$

Let σ_{K_η} and σ_{K_τ} be the standard deviations of the random variables K_η and K_τ. Following Proposition 1 we have now to choose the value of $\mathrm{cv}_K := \mathrm{cv}_{K_\eta} = \mathrm{cv}_{K_\tau}$, and of ζ_1 and ζ_2. Since L is uniformly distributed in $[\zeta_1, \zeta_2]$, we have $m_L = (\zeta_1+\zeta_2)/2$ and $\sigma_L = (\zeta_2-\zeta_1)/(2\sqrt{3})$. Thus, one has $\zeta_1 = m_L - \mathrm{cv}_L\, m_L\,\sqrt{3}$ and $\zeta_2 = m_L + \mathrm{cv}_L\, m_L\,\sqrt{3}$. In this application, $m_L = 1\times10^{-4}\,\mathrm{m}$. The sensitivity in the mechanical response of the analyzed continuum sample with respect to cv_L and cv_K is investigated.

4.2 Strong stochastic solution of the weak formulation of the boundary value problem

In this section, first, we summarize the weak formulation of the deterministic BVP, which will be used for constructing the computational model based on the mixed finite element (FE) method. Then, we introduce stochasticity in this weak formulation yielding the random weak formulation. The strong stochastic solution of this random weak formulation will be searched. Note that such a formulation is adapted to a stochastic solver based on Monte Carlo (MC) numerical simulation that will be introduced in Subsubsection 4.2.3.

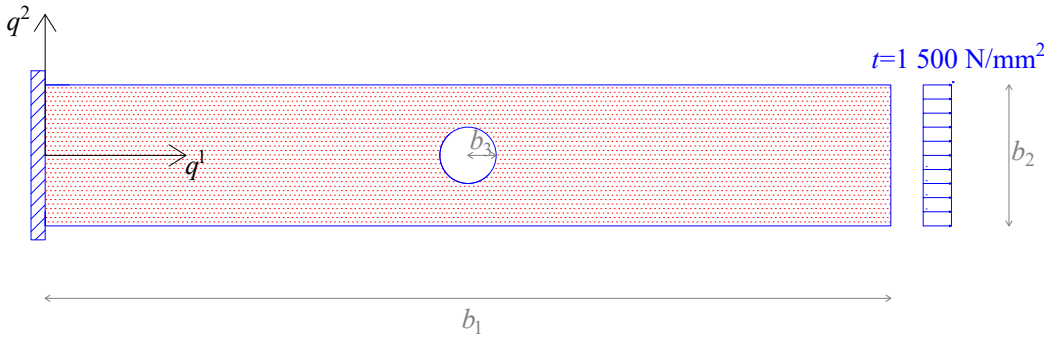

Figure 2: Numerical axial traction test on a plate made of particle-based materials with uncertainties. In the application, the constitutive parameters are the ones of concrete. In the present figure, the red points are used to underline that we are dealing with a particle-based material and, more specifically, with a composite material whose particles (or inclusions) have a random distance that is independent of the spatial and orientation directions. These assumptions on the distance between particles may be relaxed to describe more complex microstructures in which the particle-pair distance, and consequently ℓ, would depend on the spatial directions.

4.2.1 Derivation of the weak formulation of the deterministic boundary value problem

Let $\mathcal{C}_{\boldsymbol{V}}$ be the admissible space of sufficiently differentiable functions $\boldsymbol{v} : \boldsymbol{q} \mapsto \boldsymbol{v}(\boldsymbol{q})$ defined on $\mathcal{L}$ with values in $\mathbb{R}^2$ such that the trace of $\boldsymbol{v}$ is zero on the boundary $\partial\mathcal{L}_0$. Since the right-hand side of Eq. (20) exhibits the deformation tensors that are a function of $\boldsymbol{v}$ and since coefficients ξ_1 to ξ_7 depend on $\boldsymbol{x} = (\ell, k_\eta, k_\tau)$, we rewrite function $\phi(\boldsymbol{q})$ as $\widetilde{\phi}(\boldsymbol{v}, \boldsymbol{x})(\boldsymbol{q})$ in order to explicit the dependencies in $\boldsymbol{v}$ and $\boldsymbol{x}$, where $\widetilde{\phi} : (\boldsymbol{v}, \boldsymbol{x}) \mapsto \tilde{\phi}(\boldsymbol{v}, \boldsymbol{x})$ is such that $\widetilde{\phi}(\boldsymbol{v}, \boldsymbol{x})(\boldsymbol{q}) = \phi(\boldsymbol{q})$. The weak formulation of the deterministic BVP is: find $\boldsymbol{v}$ in $\mathcal{C}_{\boldsymbol{V}}$ such that

$$(\delta\pi)(\boldsymbol{v}, \delta\boldsymbol{v}; \boldsymbol{x}) = 0 \quad , \quad \forall\, \delta\boldsymbol{v} = \left\{\delta v^1, \delta v^2, \delta v^3\right\} \in \mathcal{C}_{\boldsymbol{V}} \,, \tag{54}$$

where $\delta\pi$ is the first variation of the energy functional π defined by

$$\pi(\boldsymbol{v}; \boldsymbol{x}) = \int_{\mathcal{L}} \widetilde{\phi}(\boldsymbol{v}, \boldsymbol{x})(\boldsymbol{q})\; d\boldsymbol{q} \;-\; \int_{\partial\mathcal{L}_t} t\; v^1(\boldsymbol{q})\; ds(\boldsymbol{q}), \tag{55}$$

in which $ds(\boldsymbol{q})$ is the surface element.

4.2.2 Random weak formulation and its strong stochastic solution

The random weak formulation is derived from Eqs. (54) and (55) in substituting $\boldsymbol{x}$ by the random vector $\boldsymbol{X}$ whose probability model is defined in Proposition 1. Consequently, displacement field $\boldsymbol{v}$ becomes a random displacement field $\boldsymbol{V} : \theta \mapsto \{\boldsymbol{V}(\theta) : \boldsymbol{q} \mapsto \boldsymbol{V}(\boldsymbol{q}, \theta)\}$ such that $\boldsymbol{V}(\theta)$ belongs to $\mathcal{C}_{\boldsymbol{V}}$ and configuration $\boldsymbol{r}$ becomes the random configuration function $\boldsymbol{R} : \theta \mapsto \{\boldsymbol{q} \mapsto \boldsymbol{R}(\boldsymbol{q}, \theta)\}$ defined in Section 3. The strong stochastic solution consists in finding $\boldsymbol{V}(\theta)$, for θ in Θ, with values in $\mathcal{C}_{\boldsymbol{V}}$ such that

$$(\delta\pi)(\boldsymbol{V}(\theta), \delta\boldsymbol{v}; \boldsymbol{X}(\theta)) = 0 \quad , \quad \forall\, \delta\boldsymbol{v} \in \mathcal{C}_{\boldsymbol{V}} \quad , \quad a.s. \tag{56}$$

4.2.3 Monte Carlo numerical simulation as stochastic solver

The construction of the strong stochastic solution of the random weak formulation is based on the use of the MC numerical simulation and on Eq. (56). Consequently, the steps of the stochastic solver are as follows.

1. Generation of n independent realizations $\boldsymbol{X}(\theta_1)$,...,$\boldsymbol{X}(\theta_n)$ of random variable $\boldsymbol{X}$ using the probability distribution $P_X(d\boldsymbol{x}) = p_{\boldsymbol{X}}(\boldsymbol{x})d\boldsymbol{x}$ defined in Proposition 1, in which $\boldsymbol{X} = (L, K_\eta, K_\tau)$.

2. Computation of n independent deterministic solutions $\boldsymbol{V}(\theta_1), ..., \boldsymbol{V}(\theta_n)$ that satisfy Eq. (56). In fact, the mixed FE method is used for each computation, where the displacement field and its gradient are solved both as unknowns under constraints imposed by means of Lagrange multipliers. In the formulation used, the definition of the stress tensors is not required and related issues are avoided. In this regard, one should mention the important issue of symmetry loss of the Cauchy stress tensor within the framework of second-gradient continuum models [11]. For second-gradient continuum models, details concerning the application of the mixed FE method are presented in [38]. In the presented application, the weak formulation of the equivalent continuum model is discretized using finite elements. We are simulating a particle-based material not with a random microstructure, but with random particle-pair distance between consecutive particles and random microscale stiffness parameters. As previously explained, the mesh size does not depend on the random medium properties. Although the equivalent continuum model is derived from the discrete model, this is not a classical homogenization procedure in which the microstructure is a random medium represented by apparent mechanical properties and in which the macrostructure has effective mechanical properties that are deterministic for scale separation. As a consequence, the random fluctuations of the mechanical response do not depend on the mesh size. All simulations are performed by a computing node using Intel Xeon E7-4850, in total 64 cores each with a 40 MB cache, equipped with 256 GB memory in total, running Linux Kernel 5 Ubuntu 20.04. The code is written in Python by using multithreading such that thousands of computations are distributed asynchronously to the available resources efficiently. The code in Python is wrapped by the FEniCS software into a C++ code and is solved as a compiled program. Therefore, yet efficient in developing the code in Python, the solution is highly optimized by using a massive parallelization under the current implementation. The Python code, generated during the current study, is part of the FEniCS project available at http://www.fenicsproject.org/download, and an example for the computational implementation is available in [1] to be used under the GNU Public license [24].

3. We consider a finite set of scalar observations expressed in terms of $\boldsymbol{V}$, for instance, the energy and some components of the displacement field at a given point $\boldsymbol{q}$. Let Z be the real valued-random variable representing one of the considered observations. For any fixed value n, we estimate the mean value $m_Z^{(n)}$ and the standard deviation $\sigma_Z^{(n)}$.

4. The convergence of the stochastic solver with respect to n is performed for each random variable Z by

estimating the quantity $\varepsilon_Z^{(n)} = \eta\,\sigma_Z/\sqrt{n}$ following the procedure in ([41] pp. 35) based on the central limit theorem. For that, we will plot the dimensionless quantity $\widetilde{\varepsilon}_Z^{(n)}/m_Z^{(n)}$ where $\widetilde{\varepsilon}_Z^{(n)} = \eta\,\sigma_Z^{(n)}/\sqrt{n}$.

4.3 Convergence analysis and quantification of uncertainty propagation

Let us define two points $\boldsymbol{q}_1 = (b_1/2, b_3/2, 0)$ and $\boldsymbol{q}_2 = (b_1, 0, 0)$. As a function of the number n of realization, we compute the mean value m_{Φ_1} and the standard deviation σ_{Φ_1} of the specific deformation energy in $\boldsymbol{q}_1$, where $\Phi_1 = \Phi(\boldsymbol{q}_1)$. We also evaluate the mean values $m_{V_1^1}$ and $m_{V_2^1}$ and the standard deviations $\sigma_{V_1^1}$ and $\sigma_{V_2^1}$ of the horizontal displacements at $\boldsymbol{q}_1$ and $\boldsymbol{q}_2$, where $V_1^1 = V^1(\boldsymbol{q}_1)$ and $V_2^1 = V^1(\boldsymbol{q}_2)$. Finally, we compute the mean value $m_{V_1^2}$ and the standard deviation $\sigma_{V_1^2}$ of the transversal displacement in $\boldsymbol{q}_1$, where $V_1^2 = V^2(\boldsymbol{q}_1)$. Fig. 3 displays the dimensionless quantities defined by

$$\frac{\widetilde{\varepsilon}_{\Phi_1}^{(n)}(\eta)}{m_{\Phi_1}^{(n)}} = \frac{\eta\,\sigma_{\Phi_1}^{(n)}}{\sqrt{n}\,m_{\Phi_1}^{(n)}} \quad , \quad \frac{\widetilde{\varepsilon}_{V_1^1}^{(n)}(\eta)}{m_{V_1^1}^{(n)}} = \frac{\eta\,\sigma_{V_1^1}^{(n)}}{\sqrt{n}\,m_{V_1^1}^{(n)}} \quad , \quad \frac{\widetilde{\varepsilon}_{V_2^1}^{(n)}(\eta)}{m_{V_2^1}^{(n)}} = \frac{\eta\,\sigma_{V_2^1}^{(n)}}{\sqrt{n}\,m_{V_2^1}^{(n)}} \quad , \quad \frac{\widetilde{\varepsilon}_{V_1^2}^{(n)}(\eta)}{m_{V_1^2}^{(n)}} = \frac{\eta\,\sigma_{V_1^2}^{(n)}}{\sqrt{n}\,m_{V_1^2}^{(n)}} \tag{57}$$

as a function of the number of realizations n. The value of η has been chosen equal to $\mathcal{G}^{-1}(0.95)$, $\eta = \mathcal{G}^{-1}(0.95) = 1.64$, where $\mathcal{G}$ is the standard normal cumulative distribution function. The probability of committing at most an error of 0.49 % with respect to the derived mean values was estimated to be 0.95 by considering $n = 10\,000$. The choice to analyze the mechanical response at points $\boldsymbol{q}_1$ and $\boldsymbol{q}_2$ is due to two reasons: an energy concentration occurs at $\boldsymbol{q}_1$ and the maximum displacement occurs at $\boldsymbol{q}_2$. The coefficients of variation cv_{Φ_1}, $\mathrm{cv}_{V_1^1}$, $\mathrm{cv}_{V_2^1}$, and $\mathrm{cv}_{V_1^2}$ obtained for different values of cv_L and cv_K are shown in Fig. 4. Moreover, the mean values $m_{\Delta_{\Phi_1}}$, $m_{\Delta_{V_1^1}}$, $m_{\Delta_{V_2^1}}$, $m_{\Delta_{V_1^2}}$ and the root mean square values $\mathrm{rms}_{\Delta_{\Phi_1}}$, $\mathrm{rms}_{\Delta_{V_1^1}}$, $\mathrm{rms}_{\Delta_{V_2^1}}$, $\mathrm{rms}_{\Delta_{V_1^2}}$ of the dimensionless random variables

$$\Delta_{\Phi_1} = \frac{\Phi_1 - \underline{\Phi_1}}{\underline{\Phi_1}} \quad , \quad \Delta_{V_1^1} = \frac{V_1^1 - \underline{V_1^1}}{\underline{V_1^1}} \quad , \quad \Delta_{V_2^1} = \frac{V_2^1 - \underline{V_2^1}}{\underline{V_2^1}} \quad , \quad \Delta_{V_1^2} = \frac{V_1^2 - \underline{V_1^2}}{\underline{V_1^2}} \tag{58}$$

obtained for different values of cv_L and cv_K are shown in Figs. 5 and 6, where $\underline{\Phi_1}$, $\underline{V_1^1}$, $\underline{V_2^1}$, and $\underline{V_1^2}$ are the specific deformation energy at $\boldsymbol{q}_1$, the horizontal displacements at $\boldsymbol{q}_1$ and $\boldsymbol{q}_2$, the vertical displacement at $\boldsymbol{q}_1$ corresponding to the nominal values of L, K_η and K_τ. For different values of cv_L and cv_K, Fig. 7 shows the graph of the dimensionless quantities defined by

$$\begin{aligned} \mathrm{rcv}_{\Phi_1} &= \frac{\left|\mathrm{cv}_{\Phi_1} - \mathrm{rms}_{\Delta_{\Phi_1}}\right|}{\mathrm{cv}_{\Phi_1}} \quad , \quad \mathrm{rcv}_{V_1^1} = \frac{\left|\mathrm{cv}_{V_1^1} - \mathrm{rms}_{V_1^1}\right|}{\mathrm{cv}_{V_1^1}} \\ \mathrm{rcv}_{V_2^1} &= \frac{\left|\mathrm{cv}_{V_2^1} - \mathrm{rms}_{V_2^1}\right|}{\mathrm{cv}_{V_2^1}} \quad , \quad \mathrm{rcv}_{V_1^2} = \frac{\left|\mathrm{cv}_{V_1^2} - \mathrm{rms}_{V_1^2}\right|}{\mathrm{cv}_{V_1^2}}. \end{aligned} \tag{59}$$

Equation (59) defines the relative differences between the coefficients of variation of Φ_1, V_1^1, V_2^1, V_1^2 and the coefficients of variation of the same variables that would result from replacing their means values with the nominal

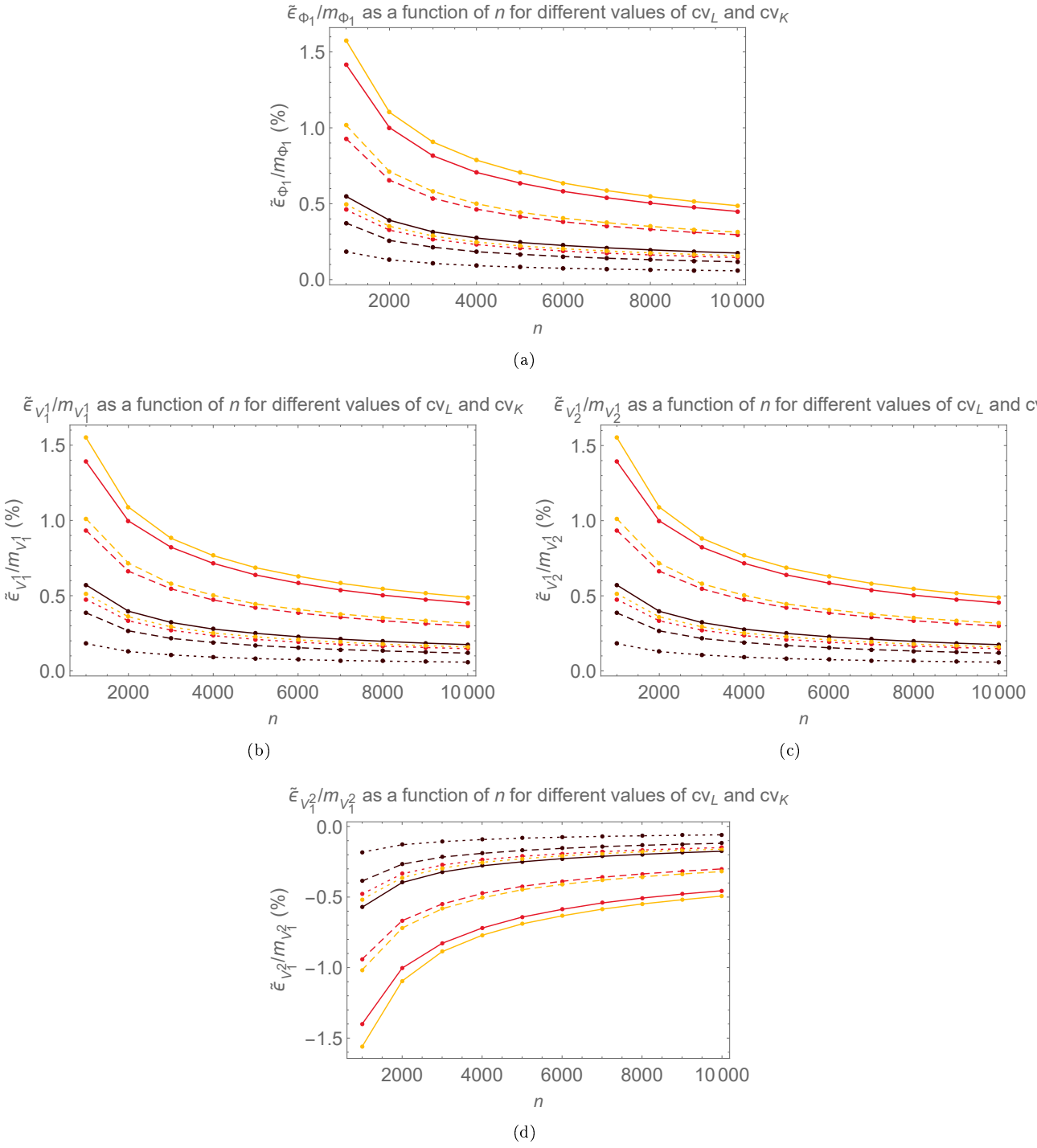

Figure 3: Graphs (a) $n \mapsto \widetilde{\varepsilon}_{\Phi_1}/m_{\Phi_1}$, (b) $n \mapsto \widetilde{\varepsilon}_{V_1^1}/m_{V_1^1}$, (c) $n \mapsto \widetilde{\varepsilon}_{V_2^1}/m_{U_2^1}$, (d) $n \mapsto \widetilde{\varepsilon}_{V_1^2}/m_{V_1^2}$ for different values of cv_L and cv_K to study the convergence with respect to n. Solid line: results for $\mathrm{cv}_L = 15\,\%$ and $\mathrm{cv}_K = 15\,\%$ (yellow), $\mathrm{cv}_L = 15\,\%$ and $\mathrm{cv}_K = 0$ (red), $\mathrm{cv}_L = 0$ and $\mathrm{cv}_K = 15\,\%$ (black). Dashed line: results for $\mathrm{cv}_L = 10\,\%$ and $\mathrm{cv}_K = 10\,\%$ (yellow), $\mathrm{cv}_L = 10\,\%$ and $\mathrm{cv}_K = 0$ (red), $\mathrm{cv}_L = 0$ and $\mathrm{cv}_K = 10\,\%$ (black). Dotted line: results for $\mathrm{cv}_L = 5\,\%$ and $\mathrm{cv}_K = 5\,\%$ (yellow), $\mathrm{cv}_L = 5\,\%$ and $\mathrm{cv}_K = 0$ (red), $\mathrm{cv}_L = 0$ and $\mathrm{cv}_K = 5\,\%$ (black).

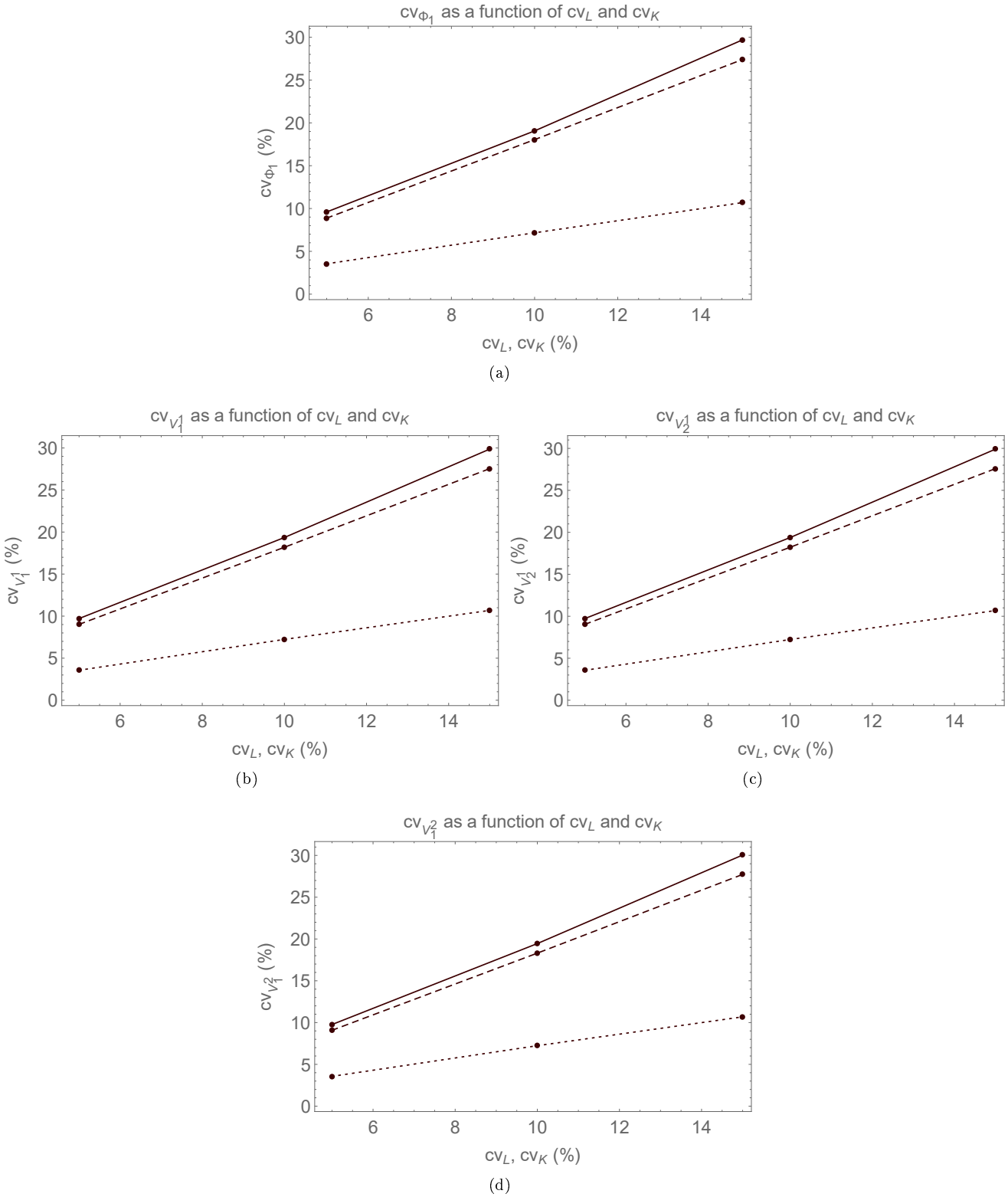

Figure 4: Graphs of (a) cv_{Φ_1}, (b) $\mathrm{cv}_{V_1^1}$, (c) $\mathrm{cv}_{V_2^1}$, (d) $\mathrm{cv}_{V_1^2}$ for different values of cv_L and cv_K. Solid line: results for cv_L equal to cv_K both different from zero. Dashed line: results for cv_L different from zero and cv_K equal to zero. Dotted line: results for cv_L equal to zero and cv_K different form zero.

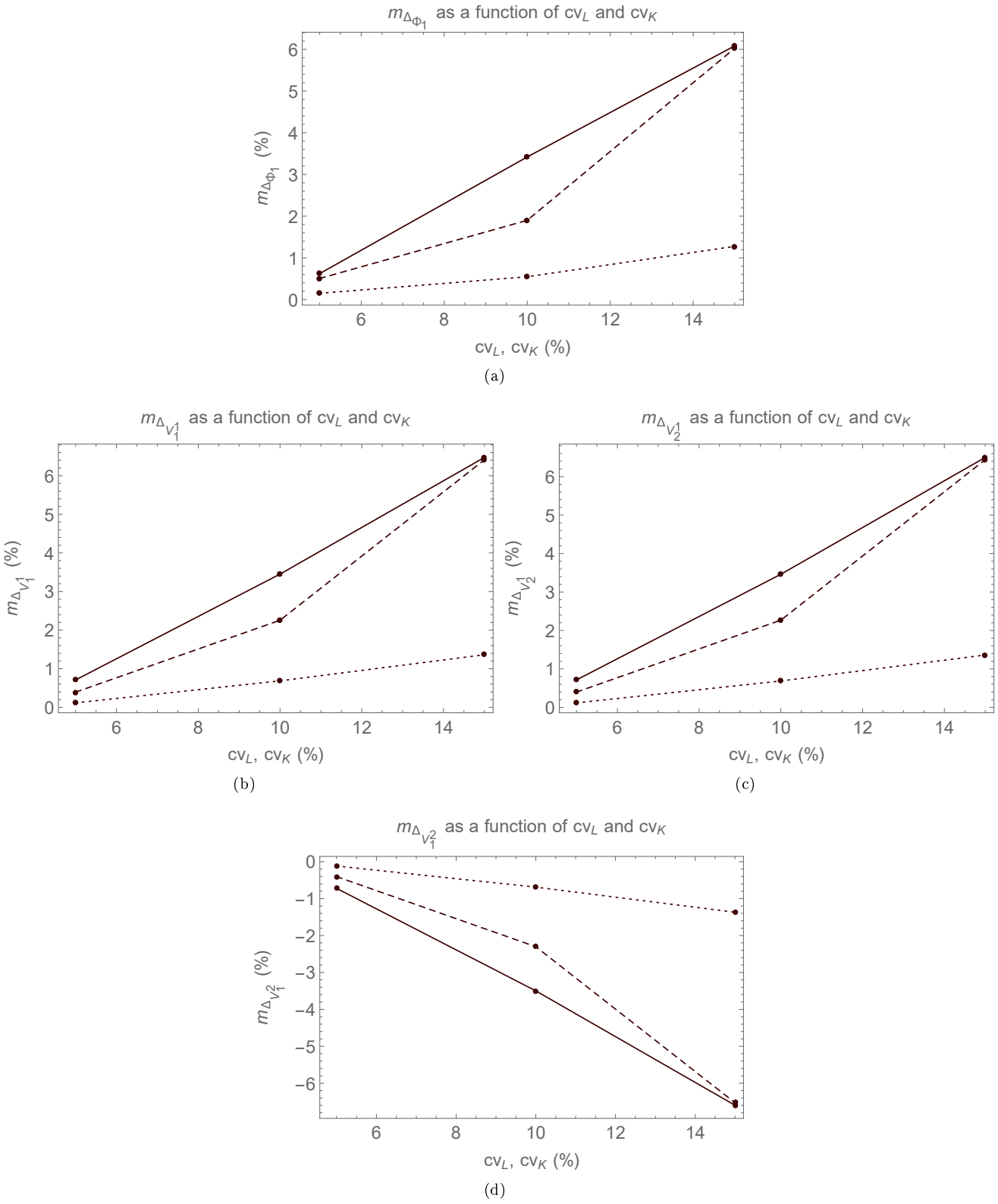

Figure 5: Graphs of (a) $m_{\Delta_{\Phi_1}}$, (b) $m_{\Delta_{V_1^1}}$, (c) $m_{\Delta_{V_2^1}}$, (d) $m_{\Delta_{V_1^2}}$ for different values of cv_L and cv_K. Solid line: results for cv_L equal to cv_K both different from zero. Dashed line: results for cv_L different from zero and cv_K equal to zero. Dotted line: results for cv_L equal to zero and cv_K different from zero.

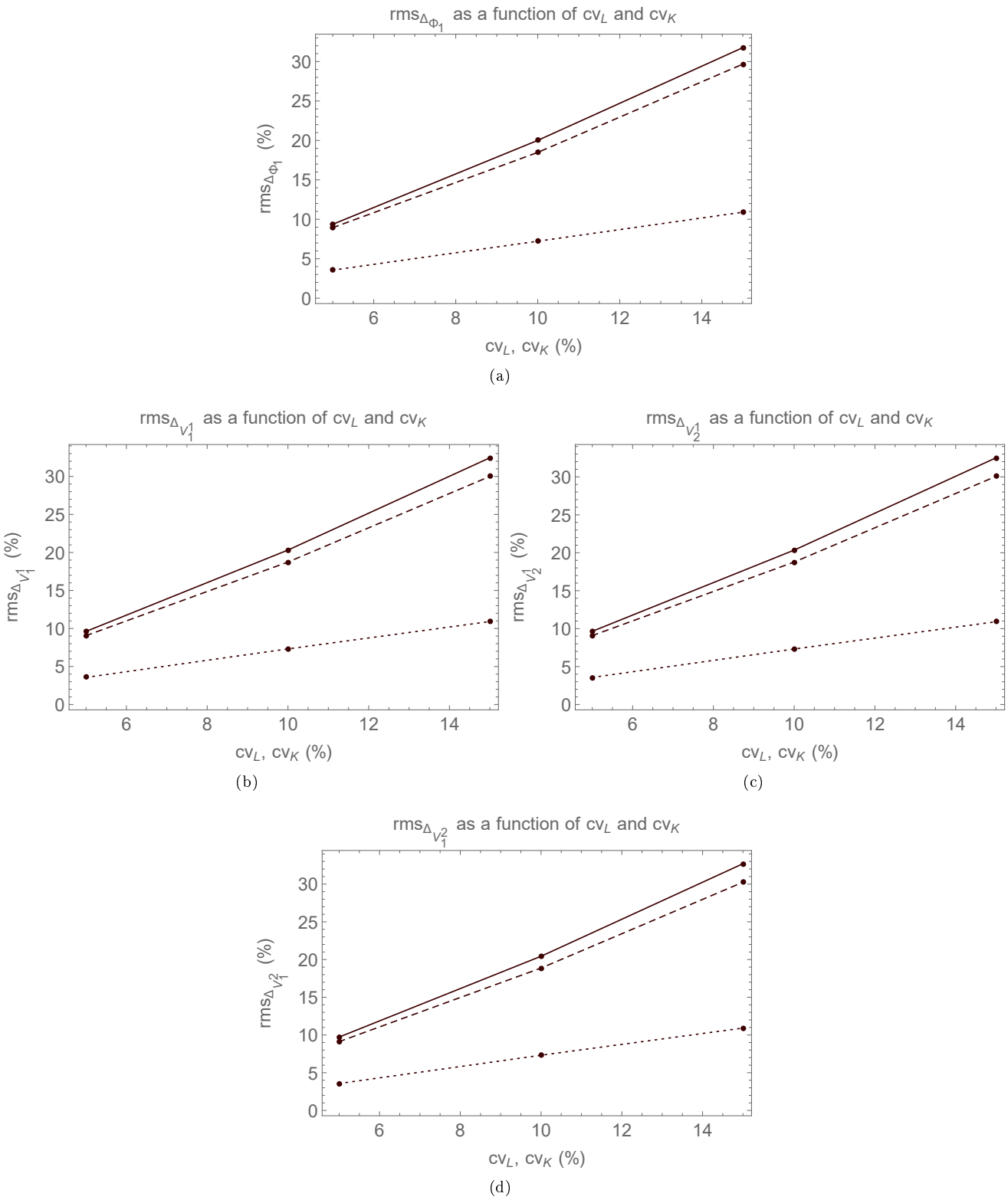

Figure 6: Graphs of (a) $\mathrm{rms}_{\Delta_{\Phi_1}}$, (b) $\mathrm{rms}_{\Delta_{V_1^1}}$, (c) $\mathrm{rms}_{\Delta_{V_2^1}}$, (d) $\mathrm{rms}_{\Delta_{V_1^2}}$ for different values of cv_L and cv_K. Solid line: results for cv_L equal to cv_K both different from zero. Dashed line: results for cv_L different from zero and cv_K equal to zero. Dotted line: results for cv_L equal to zero and cv_K different form zero.

ones.

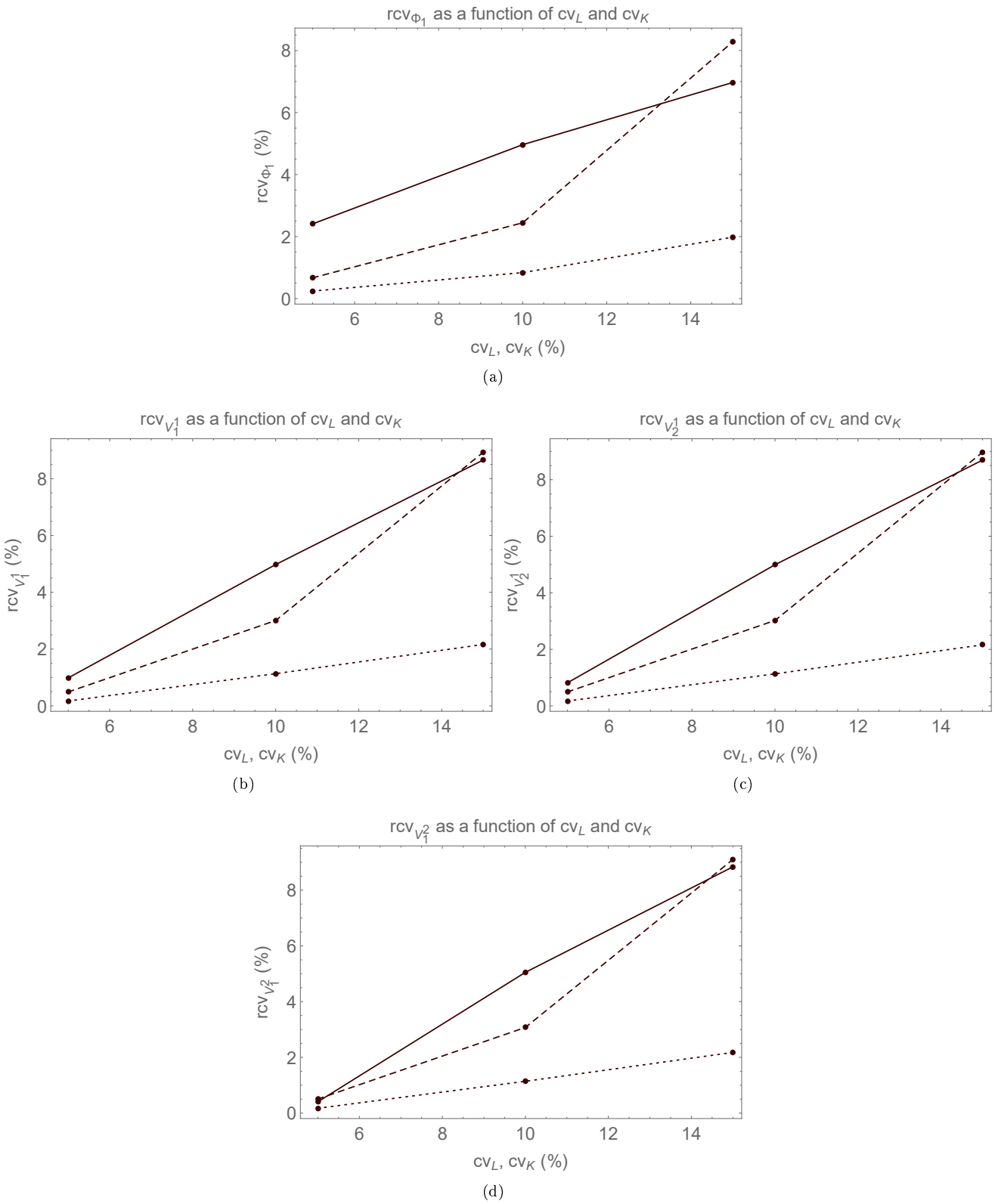

Figure 7: Graphs of (a) rcv$_{\Phi_1}$, (b) rcv$_{V_1^1}$, (c) rcv$_{V_2^1}$, (d) rcv$_{V_1^2}$ for different values of cv$_L$ and cv$_K$. Solid line: results for cv$_L$ equal to cv$_K$ both different from zero. Dashed line: results for cv$_L$ different from zero and cv$_K$ equal to zero. Dotted line: results for cv$_L$ equal to zero and cv$_K$ different form zero.

5 Conclusions

This work is the first devoted to the construction of a probabilistic model for the geometric and constitutive microscale parameters of a second-gradient model for particle-based materials. We have improved the relationship between the Cauchy deformation tensor and the second-gradient deformation tensor.

The statistical dependency between the particle-pair distance between two consecutive particles and the microscale stiffness parameters has been investigated for the micro-homogeneous and micro-isotropic continuum. A probabilistic model for these uncertain parameters has been constructed using the maximum entropy (MaxEnt) principle. Using the MaxEnt principle with the available information, it has been shown that the three considered uncertain parameters are statistically independent. The particle-pair distance between two consecutive particles is uniformly distributed, the microscale stiffness parameters are Gamma-distributed.

For the considered application, it has been shown that the random mechanical response, such as the specific deformation energy and displacements at some points, exhibits nonnegligible statistical fluctuation with respect to the level of uncertainties. It has been observed that the statistical fluctuations of the random mechanical responses are more influenced by the level of uncertainties of the particle-pair distance between two consecutive particles.

6 Acknowledgments

The first author of the paper would like to thank the Laboratoire Modélisation et Simulation Multi Echelle (MSME), Université Gustave Eiffel, where he is currently a visiting PhD student under the supervision of Prof. C. Soize.

References

[1] Abali, B.E., 2023. Supply code for computations. doi:http://bilenemek.abali.org/.

[2] Abali, B.E., Müller, W.H., Eremeyev, V.A., 2015. Strain gradient elasticity with geometric nonlinearities and its computational evaluation. Mechanics of Advanced Materials and Modern Processes 1, 1–11. doi:https://doi.org/10.1186/s40759-015-0004-3.

[3] Alibert, J.J., Seppecher, P., dell'Isola, F., 2003. Truss modular beams with deformation energy depending on higher displacement gradients. Mathematics and Mechanics of Solids 8, 51–73. doi:https://doi.org/10.1177/1081286503008001658.

[4] Altan, B.S., Aifantis, E.C., 1997. On some aspects in the special theory of gradient elasticity. Journal of the Mechanical Behavior of Materials 8, 231–282. doi:https://doi.org/10.1515/JMBM.1997.8.3.231.

[5] Altenbach, H., Eremeyev, V.A., 2013. Generalized Continua from the Theory to Engineering Applications. Springer, Vienna. doi:https://doi.org/10.1007/978-3-7091-1371-4.

[6] Altenbach, J., Altenbach, H., Eremeyev, V.A., 2010. On generalized cosserat-type theories of plates and shells: a short review and bibliography. Archive of Applied Mechanics volume 80, 73–92. doi:https://doi.org/10.1007/s00419-009-0365-3.

[7] Bažant, Z.P., 1976. Instability, ductility, and size effect in strain-softening concrete. Journal of the Engineering Mechanics Division 102, 331–334. doi:https://doi.org/10.1061/JMCEA3.0002111.

[8] Bažant, Z.P., Belytschko, T., Chang, T.P., 1984. Continuum theory for strain-softening. Journal of Engineering Mechanics 110, 1666–1692. doi:https://doi.org/10.1061/(ASCE)0733-9399(1984)110:12(1666).

[9] Bažant, Z.P., Pijaudier-Cabot, G., 1988. Nonlocal continuum damage, localization instability and convergence. Journal of Applied Mechanics 55, 287–293. doi:https://doi.org/10.1115/1.3173674.

[10] Barchiesi, E., Misra, A., Placidi, L., Turco, E., 2021. Granular micromechanics-based identification of isotropic strain gradient parameters for elastic geometrically nonlinear deformations. Zeitschrift für angewandte Mathematik und Mechanik 101, e202100059–1–21. doi:https://doi.org/10.1002/zamm.202100059.

[11] Bardet, J., Vardoulakis, I., 2001. The asymmetry of stress in granular media. International Journal of Solids and Structures 38, 353–367. doi:https://doi.org/10.1016/S0020-7683(00)00021-4.

[12] Berkache, K., Deogekar, S., Goda, I., Picu, R.C., Ganghoffer, J.F., 2017. Construction of second gradient continuum models for random fibrous networks and analysis of size effects. Composite Structures 181, 347–357. doi:https://doi.org/10.1016/j.compstruct.2017.08.078.

[13] Ciallella, A., 2020. Research perspective on multiphysics and multiscale materials: a paradigmatic case. Continuum Mechanics and Thermodynamics 32, 527–239. doi:https://doi.org/10.1007/s00161-020-00894-0.

[14] Cosserat, E., Cosserat, F., 1909. Théorie des corps déformables. Nature 81, 67. doi:https://doi.org/10.1038/081067a0.

[15] dell'Isola, F., Andreaus, U., Cazzani, A., et al., 2019. The complete works of Gabrio Piola: Volume II. Springer, Cham. doi:https://doi.org/10.1007/978-3-319-70692-4.

[16] dell'Isola, F., Andreaus, U., Placidi, L., 2015. At the origins and in the vanguard of peridynamics, non-local and higher-gradient continuum mechanics: An underestimated and still topical contribution of Gabrio Piola. Mathematics and Mechanics of Solids 20, 887–928. doi:https://doi.org/10.1177/1081286513509811.

[17] dell'Isola, F., Giorgio, I., Pawlikowski, M., Rizzi, N.L., 2016a. Large deformations of planar extensible beams and pantographic lattices: heuristic homogenization, experimental and numerical examples of equilibrium. Proceedings of the Royal Society A: Mathematical, Physical and Engineering Sciences 472, 20150790. doi:https://doi.org/10.1098/rspa.2015.0790.

[18] dell'Isola, F., Maier, G., Perego, U., et al., 2016b. The complete works of Gabrio Piola: Volume I. Springer, Cham. doi:https://doi.org/10.1007/978-3-319-00263-7.

[19] dell'Isola, F., Seppecher, P., 1995. The relationship between edge contact forces, double force and interstitial working allowed by the principle of virtual power. Comptes Rendus de l'Academie de Sciences-Serie IIb: Mecanique, Physique, Chimie, Astronomie 321, 303–308.

[20] dell'Isola, F., Seppecher, P., 1997. Edge contact forces and quasi-balanced power. Meccanica 32, 33–52. doi:https://doi.org/10.1023/A:1004214032721.

[21] Eremeyev, V.A., Lebedev, L.P., Altenbach, H., 2013. Foundations of micropolar mechanics. Springer, Berlin. doi:https://doi.org/10.1007/978-3-642-28353-6.

[22] Eringen, A.C., Edelen, D.G.B., 1972. On nonlocal elasticity. International Journal of Engineering Science 10, 233–248. doi:https://doi.org/10.1016/0020-7225(72)90039-0.

[23] Fuschi, P., Pisano, A.A., Polizzotto, C., 2019. Size effects of small-scale beams in bending addressed with a strain-difference based nonlocal elasticity theory. International Journal of Mechanical Sciences 151, 661–671. doi:https://doi.org/10.1016/j.ijmecsci.2018.12.024.

[24] GNU Public, . Gnu general public license. doi:http://www.gnu.org/copyleft/gpl.html.

[25] Greco, L., Cuomo, M., 2016. An isogeometric implicit G1 mixed finite element for Kirchhoff space rods. Computer Methods in Applied Mechanics and Engineering 298, 325–349. doi:https://doi.org/10.1016/j.cma.2015.06.014.

[26] Green, A.E., Rivlin, R.S., 1964. Multipolar continuum mechanics. Archive for Rational Mechanics and Analysis 17, 113–147. doi:https://doi.org/10.1007/BF00253051.

[27] Guilleminot, J., Soize, C., 2013. On the statistical dependence for the components of random elasticity tensors exhibiting material symmetry properties. Journal of Elasticity 111, 109–130. doi:https://doi.org/10.1007/s10659-012-9396-z.

[28] Kröner, E., 1967. Elasticity theory of materials with long range cohesive forces. International Journal of Solids and Structures 3, 731–742. doi:https://doi.org/10.1016/0020-7683(67)90049-2.

[29] La Valle, G., Ciallella, A., Falsone, G., 2022. The effect of local random defects on the response of pantographic sheets. Mathematics and Mechanics of Solids 27, 2147–2169. doi:https://doi.org/10.1177/10812865221103482.

[30] Lam, D.C.C., Yang, F., Chong, A.C.M., Wang, J., Tong, P., 2003. Experiments and theory in strain gradient elasticity. Journal of the Mechanics and Physics of Solids 51, 1477–1508. doi:https://doi.org/10.1016/S0022-5096(03)00053-X.

[31] Manzari, M.T., 2004. Application of micropolar plasticity to post failure analysis in geomechanics. International Journal for Numerical and Analytical Methods in Geomechanics 28, 1011–1032. doi:https://doi.org/10.1002/nag.356.

[32] Misra, A., Placidi, L., dell'Isola, F., Barchiesi, E., 2021. Identification of a geometrically nonlinear micromorphic continuum via granular micromechanics. Zeitschrift für angewandte Mathematik und Physik 72, 157–1–21. doi:https://doi.org/10.1007/s00033-021-01587-7.

[33] Mohan, L.S., Nott, P.R., Rao, K.K., 2002. A frictional Cosserat model for the slow shearing of granular materials. Journal of Fluid Mechanics 457, 377–409. doi:https://doi.org/10.1017/S0022112002007796.

[34] Ostoja-Starzewski, M., 1993. Random fields and processes in mechanics of granular materials. Mechanics of Materials 16, 55–64. doi:https://doi.org/10.1016/0167-6636(93)90027-0.

[35] Pietraszkiewicz, W., Eremeyev, V.A., 2009. On natural strain measures of the non-linear micropolar continuum. International Journal of Solids and Structures 46, 774–787. doi:https://doi.org/10.1016/j.ijsolstr.2008.09.027.

[36] Placidi, L., Barchiesi, E., Misra, A., Timofeev, D., 2021. Micromechanics-based elasto-plastic–damage energy formulation for strain gradient solids with granular microstructure. Continuum Mechanics and Thermodynamics 33, 2213–2241. doi:https://doi.org/10.1007/s00161-021-01023-1.

[37] Reda, H., Berkache, K., Ganghoffer, J.F., Lakiss, H., 2020. Dynamical properties of random fibrous networks based on generalized continuum mechanics. Waves in random and complex media 30, 27–53. doi:https://doi.org/10.1080/17455030.2018.1478468.

[38] Shekarchizadeh, N., Abali, B.E., Bersani, A.M., 2022. A benchmark strain gradient elasticity solution in two-dimensions for verifying computational approaches by means of the finite element method. Mathematics and Mechanics of Solids 27, 2218–2238. doi:https://doi.org/10.1177/10812865221114336.

[39] Soize, C., 2000. A nonparametric model of random uncertainties for reduced matrix models in structural dynamics. Probabilistic Engineering Mechanics 15, 277–294. doi:https://doi.org/10.1016/S0266-8920(99)00028-4.

[40] Soize, C., 2001. Maximum entropy approach for modeling random uncertainties in transient elastodynamics. The Journal of the Acoustical Society of America 109, 1979–1996. doi:https://doi.org/10.1121/1.1360716.

[41] Soize, C., 2017. Uncertainty Quantification. Springer, New York. doi:https://doi.org/10.1007/978-3-319-54339-0.

[42] Spagnuolo, M., Yildizdag, M.E., Andreaus, U., Cazzani, A., 2021. Are higher-gradient models also capable of predicting mechanical behavior in the case of wide-knit pantographic structures? Mathematics and Mechanics of Solids 26, 18–29. doi:https://doi.org/10.1177/1081286520937339.

[43] Timofeev, D., Barchiesi, E., Misra, A., Placidi, L., 2021. Hemivariational continuum approach for granular solids with damage-induced anisotropy evolution. Mathematics and Mechanics of Solids 26, 738–770. doi:https://doi.org/10.1177/1081286520968149.

[44] Turco, E., Rizzi, N.L., 2016. Pantographic structures presenting statistically distributed defects: Numerical investigations of the effects on deformation fields. Mechanics Research Communications 77, 65–69. doi:https://doi.org/10.1016/j.mechrescom.2016.09.006.

[45] Yang, F., Chong, A.C.M., Lam, D.C.C., Tong, P., 2002. Couple stress based strain gradient theory for elasticity. Journal of the Mechanics and Physics of Solids 39, 2731–2743. doi:https://doi.org/10.1016/S0020-7683(02)00152-X.